Title

Retinoic acid-dependent loss of synaptic output from bipolar cells impairs visual information processing in inherited retinal degeneration.

Author List

Logan Ganzen[1†], Shubhash Chandra Yadav[1†], Mingxiao Wei[1], Hong Ma[1], Scott Nawy[1], Richard H Kramer[1]

1. University of California Berkeley, Department of Molecular and Cell Biology. Berkeley, CA, USA

† Authors contributed equally to this work.

Corresponding Author: rhkramer@berkeley.edu

Abstract

In retinitis pigmentosa (RP), rod and cone photoreceptors degenerate, depriving downstream neurons of light-sensitive input, leading to vision impairment or blindness. Although downstream neurons survive, some undergo morphological and physiological remodeling. Bipolar cells (BCs) link photoreceptors, which sense light, to retinal ganglion cells (RGCs), which send information to the brain. While photoreceptor loss disrupts input synapses to BCs, whether BC output synapses remodel has remained unknown. Here we report that synaptic output from BCs plummets in RP mouse models of both sexes owing to loss of voltage-gated Ca^{2+} channels. Remodeling reduces the reliability of synaptic output to repeated optogenetic stimuli, causing RGC firing to fail at high stimulus frequencies. Fortunately, functional remodeling of BCs can be reversed by inhibiting the retinoic acid receptor (RAR). RAR inhibitors targeted to BCs present a new therapeutic opportunity for mitigating detrimental effects of remodeling on signals initiated either by surviving photoreceptors or by vision-restoring tools.

Significance Statement

Photoreceptor degenerative disorders such as retinitis pigmentosa (RP) and age-related macular degeneration (AMD) lead to vision impairment or blindness. Vision mediated by surviving photoreceptors or artificial vision restoration technologies, rely on bipolar cells retaining normal function despite photoreceptor death. We find that in two animal models of RP, synaptic transmission from both rod and cone bipolar cells is severely impaired owing to diminished voltage-gated calcium current, preventing postsynaptic amacrine cells and retinal ganglion cells from properly receiving and encoding visual information. We find that an inhibitor of the retinoic acid receptor restores both the calcium current and synaptic release from bipolar cells. These discoveries about bipolar cells reveal a new functional deficit in blindness and a potential therapeutically important solution.

Introduction

30 Rod and cone photoreceptors degenerate in retinitis pigmentosa (RP) and age-related macular degeneration (AMD),
31 depriving the visual system of light-evoked signals necessary for sight. The remaining retinal neurons can survive long
32 after the rods and cones are gone. Critically, retinal ganglion cells (RGCs), the output neurons of the retina, remain
33 connected to the brain (Medeiros and Curcio, 2001; Mazzoni et al., 2008). This enables responses initiated by surviving
34 photoreceptors to remain detectable late into disease progression (Ellis et al., 2023). The maintained connectivity of
35 RGCs provides a lifeline for restoring vision in profound blindness, either by regenerating lost photoreceptors from stem
36 cells, or by conferring artificial light sensitivity into surviving retinal neurons with optoelectronic (Humayun et al., 2012),
37 optogenetic (Bi et al., 2006; Sahel et al., 2021), or opto-pharmacological tools (Polosukhina et al., 2012; Tochitsky et al.,
38 2014). Whether direct or indirect, if a light stimulus can alter RGC firing appropriately, the response should be
39 transmitted to the brain and result in visual perception.

40 Unfortunately, downstream neurons undergo remodeling that can corrupt the proper encoding of information and
41 exacerbate vision loss (Telias et al., 2022). Morphological remodeling can require months to develop in mice (Pfeiffer et
42 al., 2020), while, in contrast, physiological remodeling begins almost immediately when photoreceptors die (Stasheff et
43 al., 2011; Telias et al., 2019). Many RGCs become hyperactive, spontaneously firing bursts of action potentials that
44 obscure responses initiated by surviving photoreceptors. Patch clamp recordings show that the intrinsic electrical
45 properties of RGCs are altered by photoreceptor degeneration (Tochitsky et al., 2014) and transcriptional analysis shows
46 altered expression of voltage-gated ion channels (Tochitsky et al., 2016). In addition, the plasma membrane of RGCs
47 exhibits increased permeability to large dye molecules and azobenzene photoswitches, events attributed to increased
48 expression of ATP-gated P2X receptors, which have a large pore (Tochitsky et al., 2016).

49 How does photoreceptor death in the outer retina lead to physiological remodeling of RGCs in the inner retina? We
50 found that retinoic acid (RA) is the key signal that triggers RGC hyperactivity and hyperpermeability (Telias et al., 2019).
51 Inhibitors of retinaldehyde dehydrogenase (RALDH), the enzyme that synthesizes RA, or RAR, the nuclear retinoic acid
52 receptor, reduce hyperactivity and hyperpermeability. These agents also unmask responses of RGCs to dim light,
53 sharpen responses of visual cortical neurons to patterns of illumination, and improve behavioral visual perception in
54 vision-impaired mice with partial photoreceptor degeneration (Telias et al., 2022).

55 Bipolar cells (BCs) are located between photoreceptors and RGCs. During photoreceptor degeneration, synapses onto
56 BCs exhibit morphological remodeling. BC dendrites, which normally invaginate the synaptic terminals of rods and
57 cones, begin to retract (Marc et al., 2003), disconnecting the input synapse. Synaptic input is also impaired by the loss or
58 redistribution of dendritic mGluR6 receptors (Dunn, 2015) and TRPM1 channels (Gayet-Primo and Puthussery, 2015),
59 which normally underlie the ON-BC response to the photoreceptor neurotransmitter glutamate. In addition, the
60 expression of certain voltage-gated potassium channels is misregulated in degenerated retina (Schilardi and Kleinlogel,
61 2022; Schilardi et al., 2023). Despite these negative consequences, the retina shows resilience by employing
62 mechanisms that partially compensate for photoreceptor loss. Over time, new dendrites sprout from BCs and can re-

63 establish synaptic connections in retinas with degenerated photoreceptors (Lin et al., 2012). Experimental ablation of
64 half of the rods in adults rebalances excitatory and inhibitory synaptic strength to BCs to restore proper RGC responses
65 (Care et al., 2019). In young mice, partial ablation of cones leads to dendritic rewiring in certain BCs to restore the
66 original number of input synapses (Shen et al., 2020).

67 In contrast, the question of whether BC output synapses are changed by photoreceptor degeneration has remained
68 unanswered. This is critical, as changes in BC output will alter the response properties of downstream RGCs, the only cell
69 type that provides visual input to the brain. Here we evaluate the effects of photoreceptor degeneration on output
70 synapses of two types of ON-BCs; rod bipolar cells (RBC), critical for scotopic vision and the most numerous BC type in
71 mouse, and cone bipolar cell type-6 (CBC6), which plays a crucial role in all vision, from scotopic, to mesopic, to
72 photopic. We find a dramatic reduction of voltage-gated Ca^{2+} current and neurotransmitter release from both RBCs and
73 CBC6s, weakening synaptic output and decreasing the frequency response of the BC to RGC synapse. These effects can
74 be reduced by inhibiting RA signaling, providing a potential therapeutic approach for abrogating the detrimental effects
75 of BC remodeling in RP and AMD.

76 Materials and Methods

77 **Animals**

78 Mice were handled in accordance with protocols approved by the UC Berkeley Institutional Animal Care and Use
79 Committee (AUP-2016-04-8700-1) and conformed to the NIH Guide for the Care and Use of Laboratory Animals.
80 C3H/HeJ mice (Jackson 000659) were used as the rd1 model (*Pde6b*^{rd1}). B6.CXB1-Pde6b^{rd10}/J mice were used as the rd10
81 model (Jackson 004297). CCK-ires-Cre knock-in mice (Jackson 012706, abbreviated CCK-Cre) were used to drive Cre
82 recombinase under the cholecystokinin promoter to label CBC6 cells. BAC-Pcp2-IRES-Cre mice (Jackson 010536,
83 abbreviated Pcp2-Cre) were used to drive Cre recombinase under the Pcp2 promoter to label RBCs. Ai32 mice (Jackson
84 024109, B6.Cg-*Gt(ROSA)26Sor*$^{tm32(CAG-COP4*H134R/EYFP)Hze}$/J) were used to drive channelrhodopsin-2/eYFP fusion protein in
85 Cre-expressing CBC6 or RBC cells. Both rd1 and rd10 mice strains were homozygous for their respective mutations in the
86 *Pde6b* locus. The CCK-Cre, Pcp2-Cre, and Ai32 alleles were always used in mice in a hemizygous state. Mice of both sexes
87 were used interchangeably. For experiments with WT and rd1 mice, animals were used within 3 days of postnatal day 60
88 (p60). For experiments with rd10 mice, animals were used within 3 days of p90.

89 **Retinal Dissection**

90 Mice were euthanized via isoflurane exposure and internal decapitation. Retinal dissection was performed with
91 enucleated eyes in oxygenated ACSF (in mM: 119 NaCl, 26.2 $NaHCO_3$, 11 Dextrose, 2.5 KCl mM, 1 K_2HPO_4, 1.3 $MgCl_2$*
92 $6H_2O$, 2.5 $CaCl_2$, 293 mOsm/Kg), (5% CO_2/95% O_2) in room light conditions with a dissection microscope. For retinal flat-
93 mount experiments, retinas were flattened with 4 relieving cuts. For retinal slice experiments, flattened retinas were

94 mounted on 13 mm diameter 0.45 µm filter paper discs (MF-Millipore) and sliced to a thickness of 250 µm with a
95 Stoelting Tissue Slicer. Retinal slices were rotated 90 degrees and mounted within a vacuum grease well.

96 **Electrophysiology**

97 All RGC recordings were performed in flat-mount retinas. Recordings taken from BCs and AII amacrine cells were
98 performed in retinal slices. For RGC recordings, retinas were isolated and incubated in ACSF containing hyaluronidase
99 (9,800 U/mL) and collagenase (2,500 U/mL) for 10 minutes to facilitate penetrating of the inner limiting membrane
100 allowing access to RGC somas for patch clamp recording (Schmidt and Kofuji, 2011). Retinas were mounted ganglion cell
101 side up in a recording chamber and held in place with a harp (Warner Instruments), superfused with ACSF oxygenated
102 with 5% CO_2/95% O_2 at a rate of 5 ml/minute at 34 degrees C and viewed under DIC optics with an upright microscope
103 (Olympus). Reagents for ACSF were purchased from Fisher Scientific. ON α-RGCs did not visually express ChR2-eYFP in
104 the CCK-ires-Cre mouse x Ai32 mouse lines. EPSCs from ON α-RGCs were completely blocked with the AMPAR antagonist
105 DNQX. EPSCs also had a delay from light flash to onset of about 6 ms. Other RGCs, that were not ON α-RGCs, expressed
106 ChR2-eYFP that exhibited near instantaneous current with light flash with a delay of about 0.2 ms which was insensitive
107 to DNQX.

108 For retinal slice experiments, slices were made as described and perfused in the same way as flat-mount retinas. For
109 direct recording from RBCs, ACSF $CaCl_2$ was substituted with equimolar $BaCl_2$ to prevent Ca^{2+}-activated chloride currents
110 from ANO1 channels (Paik et al., 2020). Electrodes were made with boroscilicate capillary glass tubing with OD = 1.5
111 mm, ID = 1.17 mm (Warner G150TF-4). For RGC recording, glass was pulled to a resistance of 5-6 MΩs using a Narishige
112 pipette puller. For BCs and amacrine cell recording, electrodes were made with a resistance of 7-8 MΩs with a Sutter
113 Instruments P1000. For voltage clamp experiments, the pipette solution contained (in mM): 123 Cs gluconate, 8 NaCl, 1
114 $CaCl_2$, 10 EGTA, 10 HEPES, 10 glucose, 5 Mg^{2+} ATP, 5 QX 314 (Tocris Bioscience), 0.01 Alexa 594, pH 7.4 with CsOH, 293
115 mOsm/Kg. For current clamp experiments in BCs to measure optogenetic responses, the pipette solution contained (in
116 mM): 125 K^+ Gluconate, 10 EGTA, 10 KCl, 10 HEPES, 4 Mg^{2+} ATP, 0.01 Alexa 594, 293 mOsm/Kg. Alexa Fluor 594
117 Hydrazide (ThermoFisher Scientific) at 10 µM was used to dye fill all cells during recording for confirmation of cell
118 identity. Whole-cell recordings were sampled at 20 kHz and filtered at 2 kHz with a Multiclamp 700B amplifier, digitized
119 with a 1440a or 1550a Digidata A-D converter and analyzed offline with Axograph X or Clampfit. Recordings with series
120 resistance above 10% of the cell membrane resistance or reached above 30 mΩ were discarded.

121 To block photoreceptor responses to light, the kainate receptor antagonist ACET (1 µM) and the mGluR6 agonist L-AP4
122 (10 µM) were added to ACSF. Gabazine (10 µM) and strychnine (10 µM) were also added to block ionotropic GABA and
123 glycine receptors. MFA (100 µM) was used to inhibit gap junctions. Pharmacological agents were purchased from Tocris
124 Biosciences.

125 Optogenetic stimulation of CBC6s and RBCs was provided by a 470 nm LED delivering $2.1X10^8$ photons/s, (Lumencore or
126 CoolLED pE-4000) measured at the plane of the retina with a spectrophotometer (Thor Labs). For Fig. 2 and 6,

127 stimulation intensity was varied by changing the duration of the stimulus from 0.1 to 10 ms. Thus, the number of
128 photons delivered during the optogenetic stimulus ranged from $2.1X10^7$ (100%) to $2.1X10^5$ (1%).

129 **Mapping ON α-RGC Virtual Spatial Receptive Rield**

130 Spots of light with a 50 µm diameter were generated with a Texas Instruments Digital Light Projector (CEL1015 Light
131 Engine, Digital Light innovations) controlled with CELconductor Control Software. Briefly, an ON α-RGC was identified
132 and patch clamped as described above. The cell body was focused on with an Olympus LUMPlanFl 20x/0.5 W ∞/0
133 objective and centered within a 650 µm x 650 µm field of view. Each spot projection and simultaneous EPSC recording
134 was controlled via Digidata.

135 **Trans-Retinal Stimulation**

136 To achieve electrical trans-retinal stimulation, a custom chamber was created. A 65 mm petri dish was shaved down in
137 height and embedded within a 100 mm petri dish with RTV sealant. The 65 mm dish was elevated ~ 3 mm from the
138 bottom of the 100 mm dish. An approximately 1 mm hole was melted in the center of the 65 mm dish with a 21 gauge
139 needle. To mount a retina, a ~ 7.5 mm x 7.5 mm piece of ion-permeant dialysis membrane was placed over the 1 mm
140 hole to supply an even surface to place a flat-mount retina, RGC side up. A ~ 7.5 mm x 7.5 mm piece of flexible
141 cellophane with an ~ 1mm hole punched into the center was placed over the retina as a coverslip. The retina is then
142 sealed between the membrane and coverslip with vacuum grease so that the only electrical path between the two
143 dishes is through the retina. Two copper wires were placed in each dish below and above the retina which were
144 connected to an ISO-Flex stimulus isolation unit. Electrical stimulation was achieved by setting the desired voltage on
145 the ISO-Flex and triggering the stimulus via Digidata.

146 **2-Photon iGluSnFR Imaging**

147 2-Photon fluorescence imaging was performed on a Sutter Instruments moveable objective microscope with an Olympus
148 XLUMPlanFl 20x/0.95 W ∞/0 objective. iGluSnFR excitation was achieved with a Coherent Chameleon Ultra II tuned to
149 910 nm. Imaging was performed with ScanImage software. Scanning field of view was 25 µm x 25 µm. Images collected
150 in Fig 4c-d were scanned at 256 pixels per line x 256 lines (frame rate = 1.48 Hz, 2 ms per line). Higher time resolution of
151 iGluSnFR flouresence for Fig 4e-g was performed at 256 pixels per line x 6 lines (frame rate = 63.13 Hz, 2 ms per line).

152 **Immunohistochemistry**

153 ON α-RGCs were injected with Alexa Fluor 568 hydrazide (A10441, Thermo Fisher) as described previously (Tetenborg et
154 al., 2017). In short, somas of RGCs in the flat-mount retina were visualized by acridine orange labeling (Meyer et al.,
155 2014). Potential ON α-RGCs were identified based on their large soma size (>20 µm) and targeted with sharp
156 microelectrodes containing Alexa Fluor 568. The dye injected retinas were fixed with 4% PFA and the following
157 immunolabeling was carried out as described before (Yadav et al., 2019). In brief, the flat-mount retinas were incubated

158 into primary and secondary antibodies for 3 and 1 days, respectively. CtBP2 (mouse, AB_399431, BD Biosciences)
159 monoclonal and secretagogin (sheep, AB_2034062, BioVendor) polyclonal antibodies were used at a dilution of 1:500
160 and 1:750, respectively. All immunostainings were performed at room temperature. Images were scanned with 40x/1.4
161 oil objective using Zeiss LSM780 Laser Scanning Confocal Microscope. The z-stacks were acquired at a constant pixel size
162 of 60nm*60nm and a z-step of 0.3µm unless stated otherwise. All raw images thus obtained were deconvolved with
163 Huygens Essential software (Scientific Volume Imaging, Netherlands). The deconvolution was achieved by using a
164 theoretical point spread function. The resulting images were further processed and analyzed in Fiji (https://fiji.sc/)
165 (Schindelin et al., 2012). The z-stacks were normalized using stack histograms prior to analysis. The colocalization
166 analysis was carried out within each optical section unless stated otherwise. Brightness and contrast of the images were
167 adjusted post-analysis in Fiji.

168 Colocalization between channels was performed with Fiji utilizing the colocalization highlighter plugin as previously
169 described (Behrens et al., 2022). Briefly, deconvoluted z-stacks were segmented using stack histogram. Secretagogin and
170 CtBP2 signals were thresholded with Otsu's method, and dye injected RGCs were manually thresholded. With
171 colocalization highlighter, an intensity ratio of 50% was applied to estimate colocalization between Secretagogin and
172 CtBP2. Colocalization of Secretagogin and CtBP2 with RGCs was performed sequentially with an intensity ratio of 10%.
173 Resultant 8-bit images of puncta were generated where at least 5 or more connected voxels were considered as
174 colocalization. These images were overlayed with either RGCs or CBC6 axon terminals, and the 3D Objects Counter
175 plugin was used to quantify putative synaptic contacts. To isolate individual CBC6 axon terminals, axonal endings were
176 traced back from a common point in the z-stack 8 µm into the IPL.

177 **AAV Delivery of iGluSnFR**

178 Plasmid containing iGluSnFR(A184S) under the control of the human synapsin promoter was purchased from Addgene
179 (#106174) and packaged in the AAV8-Y733F serotype (Dalkara et al., 2013). Viral constructs were generated in the Gene
180 Delivery module of the Vision Science Core at UC Berkeley. One month prior to imaging, 1.5 µl of virus ($1x10^{15}$ vg/mL)
181 was injected into intravitreally into the eye of rd1 or WT mice.

182 **Data Visualization and Statistics**

183 All reported statistics and diagrams were generated with R 4.2.2. Retinal and experimental diagrams were created with
184 Biorender.com.

185

186 ## Results

187 **Voltage-gated calcium current in ON-BCs is reduced by photoreceptor degeneration.**

188 Calcium influx through voltage-gated Ca^{2+} channels is critical for evoking neurotransmitter release at the BC output
189 synapse (Tachibana et al., 1993). To measure the voltage-gated Ca^{2+} current, we recorded from BC somata in retinal
190 slices, a preparation that made the cells easy to identify and access with a patch pipette. After establishing whole-cell
191 voltage clamp we applied a series of depolarizing voltage steps. We compared activation of the voltage-gated Ca^{2+}
192 current in BCs from wildtype (WT) mice from those in rd1 and rd10 mice, widely used animal models of RP. We focused
193 on the Type-6 ON cone bipolar cell (CBC6), which synapses directly onto RGCs, and rod bipolar cells (RBCs), which drive
194 RGCs indirectly through a serial synapse onto the CBC output synaptic terminal (Fig. 1A,E). Candidate BCs of each type
195 were identified with cell-type selective gene promoters that drive expression of a fluorescent protein reporter fused
196 with channelrhodopsin-2 (ChR2-eYFP), namely the Cck promoter for CBC6 cells and the Pcp2 promoter for RBCs. The
197 identity of individual BCs was confirmed by dye-filling the cell to localize their terminals to specific sublamina in the
198 inner plexiform layer (IPL) (Fig. 1A,E).

199 We found that the voltage-gated Ca^{2+} current in CBC6 cells was 3-fold larger in WT mice than in rd1 or rd10 mice at
200 maximal activation (Fig.1B–D). Similarly, voltage-gated Ca^{2+} current in RBCs was 2-fold larger than in rd1 or rd10 mice at
201 maximal activation (Fig. 1F–H). In both BC types, steady-state current vs. voltage curves showed reduced current
202 amplitude without any change in voltage-dependent activation (Fig. 1C–D,G–H), consistent with a change in Ca^{2+} channel
203 number rather than a change in gating properties or channel type. We found that the L-type Ca^{2+} channel inhibitor
204 nimodipine eliminated the current in CBC6 cells consistent with previous findings that L-type Ca^{2+} channels predominate
205 in BCs (Heidelberger and Matthews, 1992). Photoreceptor degeneration occurs early in postnatal development in rd1
206 mice and later in adulthood in rd10 mice, making certain aspects of morphological remodeling more severe in the rd1
207 strain (Marc et al., 2003). Despite this, the loss of Ca^{2+} current in CBC6 cells and RBCs was nearly identical in rd1 and rd10
208 mice.

209

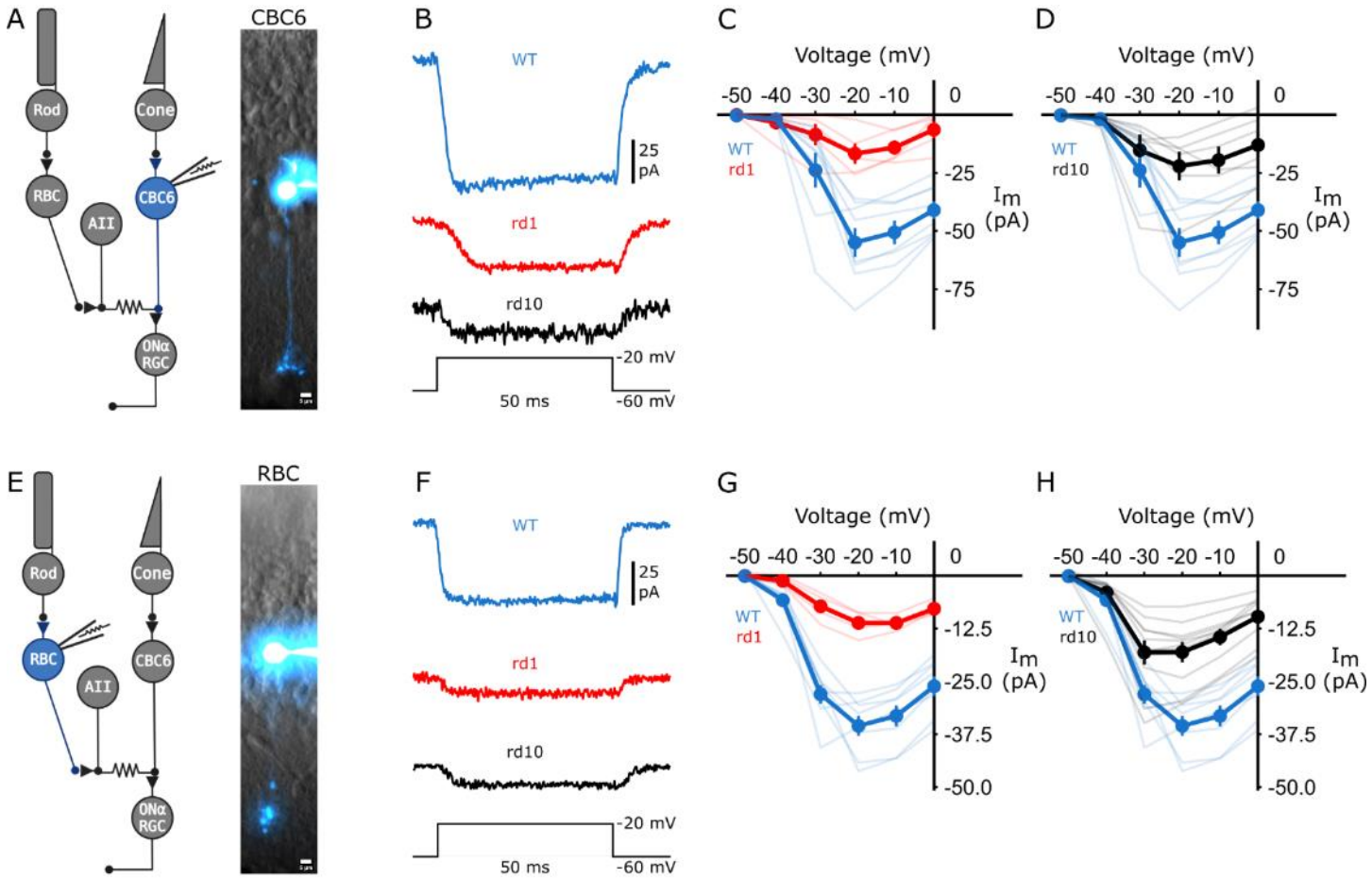

Figure 1. Voltage-gated calcium current of ON-BCs is reduced in photoreceptor degenerated retinas. A, E) Retinal circuit diagrams showing whole-cell patch-clamped CBC6 cells or RBCs with accompanying fluorescent dye fills (Alexa-Fluor 594) of a CBC6 cell or an RBC in a retinal slice. Scale bars = 5 µm. B, F) Inward calcium currents in a CBC6 and RBC from WT, rd1, and rd10 retinas. Current was activated with a depolarizing voltage step (50 ms) from -60 mV to -20 mV. C, D) Steady-state current vs. voltage (I-V) curves, elicited with a series of 10 mV incrementing depolarizing steps from -60 to 0 mV from CBC6 cells WT: N = 8 rd1: N = 6; rd10: N = 6. G, H) Steady-state current vs. voltage (I-V) curves for RBCs, WT: N = 9; rd1: N = 6; rd10: N = 10). I-V curves from rd1 and rd10 BCs shows that the voltage-gated calcium current is lower than in WT BCs (Pairwise Wilcoxon Rank Sum Exact Test (PWT) with false discovery rate (FDR) correction (for CBC6: WT – rd1, p = 0.016; WT – rd10, p = 0.048. For RBC: WT – rd1, p= 0.001; WT – rd10, p-value = 0.001). Transparent traces indicate individual cells. Error bars indicate ± SEM.

222 **Transmission at the BC output synapse is reduced by photoreceptor degeneration.**

223 Neurotransmitter release is triggered by intracellular Ca^{2+}, hence the reduced Ca^{2+} current in BCs suggests that synaptic
224 transmission will also be reduced. ON-BCs are ordinarily depolarized in the light, but in the absence of photoreceptors
225 we can use optogenetics as an alternative to depolarize the cells and evoke synaptic release. We leveraged the cell-type
226 selective expression of ChR2-eYFP to optogenetically depolarize either RBCs or CBC6s, in the WT, rd1, or rd10
227 background. To interrogate the BC output synapse in isolation, we blocked photoreceptor inputs onto BCs with the
228 mGluR6 agonist L-AP4 and the kainate receptor antagonist ACET, which together eliminate light responses in all BCs
229 (Tien et al., 2017). We also blocked inhibitory synaptic inputs onto BCs with antagonists of ionotropic GABA and glycine
230 receptors and electrical synapses with the gap junction uncoupler MFA to block inner retina oscillations.

231 We stimulated CBC6 cells with light flashes while we recorded evoked excitatory postsynaptic currents (EPSCs) from ON
232 α-RGCs in flat-mount retinas (Fig. 2A). Amongst the various BCs, the promoter for cholecystokinin (Cck) enables
233 transgene expression specifically in CBC6 cells, although sparse expression has been noted in non-BC cell types, including
234 some ON type RGCs (Zhu et al., 2014). ON α-RGCs were identified by soma size and dendritic layer termination in the
235 IPL, mapped after dye-filling. If a ChR2-eYFP expressing RGC was inadvertently targeted, it was removed from further
236 consideration based on the exceedingly short optogenetic response delay and lack of susceptibility to the AMPAR
237 antagonist DNQX (See Methods).

238 Optogenetically evoked EPSCs in ON α-RGCs were smaller and slower in rd1 and rd10 than in WT retinas (Fig. 2B). EPSCs
239 were reduced across all stimulation strengths, including stimuli that saturated the synaptic response, consistent with
240 diminished synaptic efficacy. EPSCs were ~40% smaller in rd1 and rd10 retinas with a saturating stimulus (Fig. 2C,D). In
241 addition, EPSC kinetics were slower in both rd1 and rd10, with a longer time-to-peak (Fig. 2E). The output synapse also
242 exhibited a striking loss of sensitivity in degenerated retina. The stimulus required to evoke a half-maximal EPSC was
243 nearly three times stronger in rd1 and rd10 compared to WT retina (Fig. 2F). Thus, the CBC6 output synapse exhibited a
244 decrease in both peak response and sensitivity.

245 For examining the output synapse of RBCs, we expressed ChR2-eYFP under control of the RBC-selective promoter for
246 Purkinje cell Protein-2 (Pcp2) (Liang et al., 2021). We optogenetically depolarized RBCs in retinal slices, recording EPSCs
247 in their postsynaptic partner the AII amacrine cell. AII amacrine cells are electrically coupled to CBC6, indirectly driving
248 RGC firing (Fig. 2G). We recorded EPSCs in AII cells, which were identified after dye-filling by their distinctive cell body
249 shape and dendritic terminations in the IPL. Synaptic output of RBCs onto AII cells was also reduced in rd1 and rd10
250 retinas as compared to WT (Fig. 2H). Responses to saturating light at the RBC synapse were reduced by ~75% in rd1
251 retinas and ~65% in rd10 retinas as compared to WT with a saturating stimulus (Fig. 2I,J). The output synapse of RBCs
252 also exhibited a loss of sensitivity to optogenetic stimulation, although less striking than at the CBC6 output synapse (Fig.
253 2L). RBCs ordinarily exhibit highly synchronous release, resulting in rapid and transient postsynaptic responses (Singer et
254 al., 2004), but the responses were slower to rise and more prolonged in degenerated retina, implying that degeneration

255 promotes more asynchronous transmitter release from RBCs. The time-to-peak of evoked EPSCs was 2- or 3-fold longer,
256 for rd10 and rd1 retinas as compared to WT (Fig. 2K). In summary, the output synapses of both CBC6 cells and RBCs
257 show dramatically reduced synaptic efficacy in degenerated retina, consistent with reduced Ca^{2+}-dependent
258 neurotransmitter release.

259 We were concerned that the expression of ChR2 might be lower in BCs from degenerated retinas than in BCs from WT
260 retinas, such that the same light flash might elicit less depolarizing current resulting in a deficit in synaptic release. To
261 test for this possibility, we used patch clamp recordings to compare the light-elicited ChR2 current in rd1, rd10, and WT
262 retinas (Fig. 3A). The dendritic tree of BCs regresses in degenerated retinas, so to correct for the smaller surface area we
263 measured whole-cell capacitance and calculated the current density for each cell. We found that the ChR2 current
264 density in CBC6 cells was no different in rd1 than in WT retinas (Fig. 3B,C). Similarly, the ChR2 current density in RBCs
265 was no different in rd10 retina than in WT (Fig. 3F,G). The kinetics of the light-elicited current were identical and there
266 was no difference in paired currents elicited by two light flashes, suggesting no difference in activation or inactivation
267 properties (Fig. 3 D,E). Light-elicited membrane depolarization caused by a single flash was also similar in degenerated
268 retinas as in WT (Fig. 3H-J). It should be noted that membrane potential measurements taken from the cell body
269 inaccurately reflect the membrane potential at the synaptic terminal, which is electrotonically distant. Because the WT
270 cells have a larger voltage-gated Ca^{2+} current that can amplify depolarizations, the local depolarization in the BC
271 terminals might well be larger in WT than in rd1 or rd10 terminals, even if they express the same number of ChR2
272 channels.

273

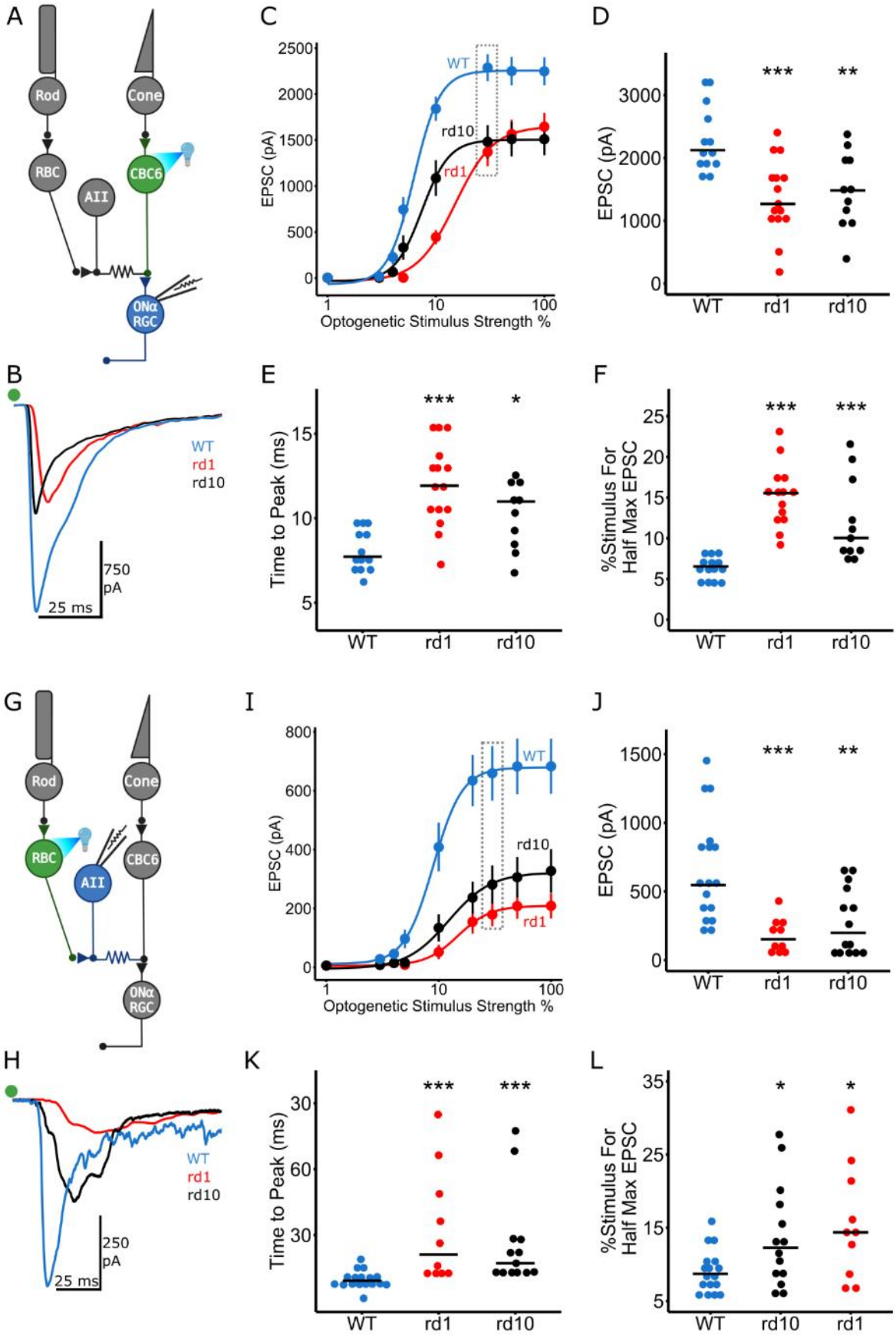
A
Rod
Cone
RBC
AII
CBC6
ONα RGC
B
WT
rd1
rd10
750 pA
25 ms
C
EPSC (pA)
Optogenetic Stimulus Strength %
D
E
Time to Peak (ms)
F
%Stimulus For Half Max EPSC
G
H
250 pA
I
J
K
L

274 %

Figure 2. Synaptic output from ON-BCs is reduced in photoreceptor degenerated retinas. A,G) Retinal circuit diagrams showing optogenetically stimulated CBC6 cells or RBCs. EPSCs were recorded from a postsynaptic ON α-RGC or AII amacrine cell, respectively. B,H) EPSCs in CBC6 cells (B) and RBCs (H). Note the reduced EPSCs in rd1 and rd10 retinas compared to WT. The green dot represents the light flash. C,I) At all effective optogenetic stimulus strengths, EPSCs from CBC6 cells (C) and RBCs (I) were smaller in rd1 and rd10 than in WT (For CBC6 cells: rd1 vs. WT: $p<0.001$; rd10 vs. WT: $p = 0.009$; rd1:N=15, rd10:N=11, WT:N=13. For RBCs: rd1 vs. WT: $p<0.001$; rd10 vs. WT: $p<0.001$; WT:N=17, rd1:N=10, rd10:N=14). D,J) EPSCs elicited by a saturating stimulus (dashed box in panels C and I) were smaller in rd1 and rd10 than in WT (For CBC6 cells: rd1= 1.27 nA, rd10 = 1.48 nA, WT = 2.12 nA; rd1 vs. WT: $p <0.001$; rd10 vs. WT: $p = 0.008$; for RBCs: rd1 = 152 pA, rd10 = 198 pA, WT = 546 pA; rd1 vs. WT: $p <0.001$; rd10 vs. WT: $p = 0.007$). E,K) Rise time of EPSCs is slower in rd1 and rd10 than in WT retinas for both the CBC6 output synapse (rd1 = 11.92 ms, rd10 = 10.99 ms, WT = 7.72 ms; rd1 vs. WT, $p <0.001$; rd10 vs. WT, $p = 0.011$) and the RBC output synapse (rd1 = 21.17 ms, rd10 = 19.19 ms, WT = 9.24 ms; rd1 vs. WT, $p <0.001$; rd10 vs. WT, $p <0.001$). F,L) The calculated stimulus strength required to elicit half-maximal EPSCs from CBC6 cells (F) and RBCs (L) is higher for rd1 and rd10 than for WT. (For CBC6 cells: rd1= 15.5%, rd10 = 10.0%, WT = 6.5%; rd1 vs. WT: $p <0.001$; rd10 vs. WT: $p <0.001$; for RBCs: rd1 = 14.3%, rd10 =12.3%, WT = 8.7%; rd1 vs. WT: $p = 0.02$; rd10 vs. WT: $p = 0.05$). For panels D – F, and J – L, each data point represents EPSC statistics from an individual recording; horizontal lines represent median EPSC values. Error bars indicate ± SEM. All statistical comparisons were made with PWT with FDR correction.

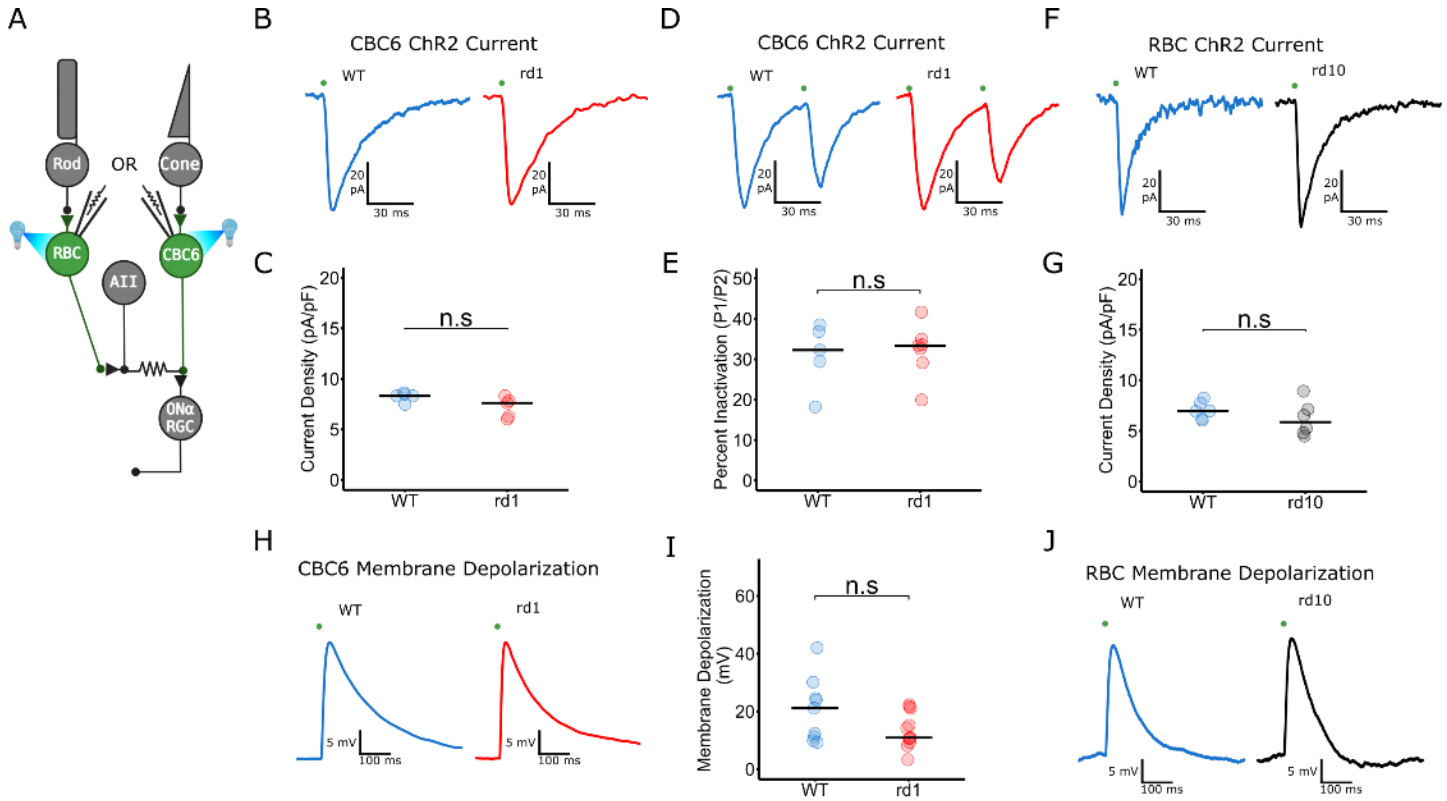

Figure 3. Intrinsic ChR2 function is not altered by photoreceptor degeneration. A) Retinal circuit diagram showing whole-cell patch-clamp and simultaneous optogenetic stimulation of a CBC6 cell or an RBC. B) ChR2-induced inward current elicited by optogenetic stimulation of CBC6 cells in WT and rd1. C) There is no difference in ChR2 current density in CBC6s in WT and rd1 retinas. WT: N=5, rd1: N=5 ($p = 0.15$). D) ChR2-induced inward current elicited in CBC6 cells by a pair of optogenetic stimuli 50 ms apart in WT and rd1. E) ChR2 current inactivated approximately 30% in the second flash with no difference between both rd1 and WT retinas. WT: N=5, rd1: N=7 ($p = 0.88$). F) ChR2-induced inward current elicited by optogenetic stimulation of RBCs in WT and rd10. G) There is no difference in ChR2 current density in RBCs in WT and rd10 retinas WT: N=6, rd1: N=6 ($p = 0.35$). H) ChR2-induced membrane depolarization in a WT and rd1 CBC6 cell. I) There was no difference in the ChR2-elicited membrane depolarization. WT: N=9, rd1: N=11 ($p = 0.11$). J) ChR2-induced membrane depolarization in a WT and rd10 RBC. CBC6 optogenetic pulse width: 2.5 ms. RBC optogenetic pulse width: 1 ms. Horizontal lines represent median values. All statistical comparisons were made with PWT with FDR correction.

308 **Morphological analysis shows that the number of output synapses from CBC6 cells is unaltered by photoreceptor**
309 **degeneration.**

310 Reduced synaptic transmission could either be caused by a decrease in the number of synaptic contacts between pre-
311 and postsynaptic neurons or by a decrease in the synaptic efficacy with no change in synapse number. To distinguish
312 between these possibilities, we used immunohistochemistry and fluorescence microscopy to quantify the density of
313 CBC6 synaptic contacts onto ON α-RGC dendrites in the IPL. We used an antibodiy against secretagogin to visualize the
314 axon terminals of CBC6 cells. Secretagogin labels CBC types 2,3,4, 5, 6 in the mouse retina. CBC2-4 are OFF-BCs that
315 terminate in distant OFF sublamina, while CBC5 stratifies in IPL 3, so CBC6 terminals can be identified unambiguously in
316 IPL 4 (Puthussery et al., 2010). CBC6 cells constitute more than 70% of bipolar synaptic inputs to ON α-RGC (Schwartz et
317 al., 2012) while other ON-CBC types sharing stratification with ON α-RGCs lack secretagogin expression (Helmstaedter et
318 al., 2013). We labeled BC synaptic ribbons with a fluorescent antibody against ribeye, the main structural protein in the
319 ribbon. Finally, we visualized the dendritic tree of an individual ON α-RGC by dye-filling the cell (Fig. 4A).

320 Confocal microscope images from the IPL show CBC6 terminals overlapping with ON α-RGC dendrites (Fig. 4B). To
321 restrict our analysis to functional synapses, we examined the overlap between ON α-RGC dendrites and ribeye-labeled
322 puncta (CtBP2) within CBC6 terminals (Fig. 4C–E). We found that the number of putative synapses onto the ON α-RGC
323 was the same in WT and rd1 retinas (Fig. 4F). The number of synapses per unit area of the ON α-RGC was also the same
324 (Fig. 4G). By focusing through the depth of the IPL, we reconstructed the terminal tree of an individual CBC6 cell, which
325 is displayed as a flattened 2D projection (Fig. 4H). Imaging ribeye puncta overlapping with the terminal tree revealed the
326 total number of presumptive ribbon synapses formed by that CBC6 cell (Fig. 4I,J). Using this approach, we found no
327 difference in the number of CBC6 cell output synapses between WT and rd1 retinas (Fig. 4K). Additionally, there was no
328 difference in the density of ribbons per axon terminal (Fig. 4L). We conclude that there is no difference in the number of
329 presumptive CBC6 synapses between WT and rd1 retina.

330

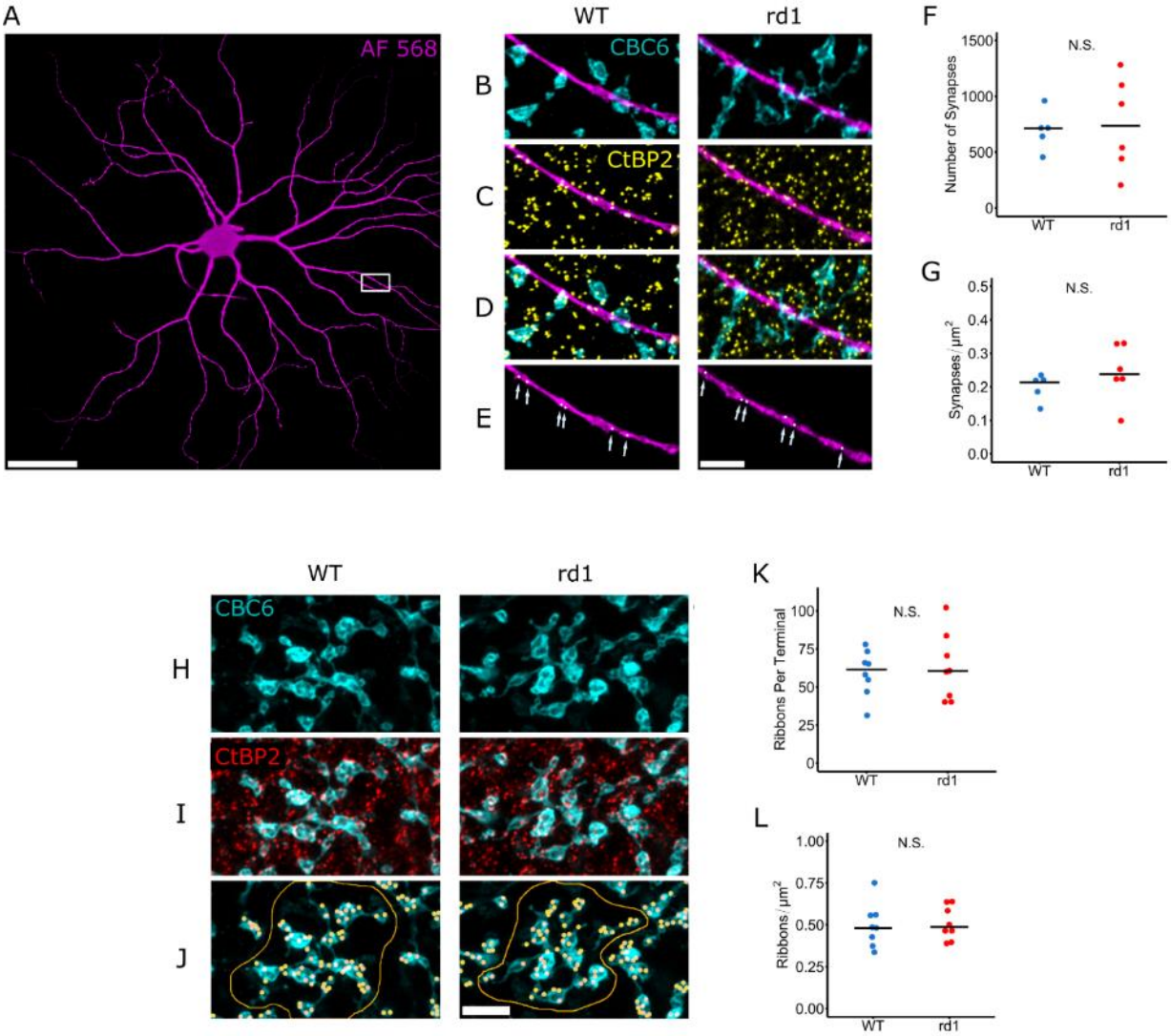

Figure 4. CBC6 cell output synapse morphology is unaltered by photoreceptor degeneration. A) Soma and dendrites of an ON α-RGC, labeled by intracellular injection with Alexa Fluor 568. Image is a 3-D projection from a stack of confocal optical sections. B-E) Magnified view of one ON α-RGC dendrite (magenta), overlapping with CBC6 axon terminals (B), labeled with anti-secretagogin (cyan), C) overlapping with synaptic ribbons, labeled with anti-CtBP2 (yellow), D) overlapping with synaptic ribbons exclusively in CBC6 terminals, identified by co-labeling with anti-secretagogin and anti-CtBP2. E) Arrows point to sites of co-localization between the dendrite, CBC6 axon terminals, and CtBP2, i.e., presumptive ribbon synapses between CBC6 cells and the ON α-RGC. F, G) Quantification of the total number of CBC6 ribbon synapses across all optical sections of the dendritic tree of an ON α-RGC (F) and the density of CBC6 ribbon synapses per unit area of the ON α-RGC. (G). There is no significant difference in the number (WT vs. rd1: $p = 1$) or density of ribbon synapses (WT vs. rd1: $p = 0.33$) in rd1 vs. WT retinas. WT: N=5, rd1: N=6. H)2D projection of the 3D structure of axon terminals of CBC6 cells in WT and rd1 retinas. I) CBC6 axon terminal overlapping with CtBP2. J) CBC6 axon terminals with yellow dots denoting thresholded points of overlap with CtBP2. The red outline indicates the axon terminal tree of one individual CBC6 cell. K, L) Quantification of the number of CtBP2 sites per CBC6 axon terminal tree (K) and the density of CtBP2 sites per CBC6 axon terminal tree (L). There is no significant difference in the number (WT vs. rd1: $p = 0.33$) or density (WT vs. rd1: $p = 1$) of ribbon synapses made by an individual CBC cell onto an ON α-RGCs in rd1 vs. WT retinas. WT: N=8, rd1: N=8. Scale bars: A (50 µm); B-E, H-J (5 µm). All statistical comparisons were made with PWT with FDR correction.

349 **Electrically evoked glutamate release from BC terminals is reduced by photoreceptor degeneration.**

350 The described results suggest that decreased synaptic efficacy from BC to postsynaptic cells in the photoreceptor-
351 degenerated retina is caused by decreased release of the neurotransmitter glutamate. To directly confirm reduced
352 glutamate release, we used the genetically encoded glutamate indicator iGluSnFR, delivered to RGCs with an AAV vector
353 that transduces diverse types of RGCs indiscriminately. After allowing 2-3 weeks for viral transduction and gene
354 expression, we isolated and mounted the retina in a chamber that enables simultaneous trans-retinal electrical
355 stimulation and 2-photon imaging (Fig. 5A). By focusing on different depths through the inner retina, we obtained virtual
356 cross-sections of the IPL, which showed similar baseline levels of iGluSnFR expression in WT and rd1 retinas (Fig. 5B). We
357 placed electrodes across the thickness of the retina to enable electrical stimulation of all cells. To examine
358 neurotransmitter release from BCs output synapse in isolation, we pharmacologically blocked all input synapses to BCs.
359 Under these conditions, we found that a brief electrical stimulus (10 ms) evoked a transient increase in iGluSnFR
360 fluorescence in the ON-layer of the IPL that was smaller in rd1 than in WT (Fig. 5C). The peak change in fluorescence
361 over background ($\Delta F/F_0$) was 75% smaller in rd1 than in WT (Fig. 5D,E). We were concerned that retinas lacking
362 photoreceptors might have altered tissue resistance, which could impact the effectiveness of electrical stimulation of
363 BCs. To address this point, we varied electrical stimulus strength to generate a range of responses, from no detectable
364 iGluSnFR signal to a saturating signal (Fig. 5F). We found that while the magnitude of the response to all stimuli
365 (including the saturating stimulus) was lower in rd1, the sensitivity was the same, indicating that the reduced response
366 could not be attributed to less effective electrical stimulation (Fig. 5F). Furthermore, peak iGluSnFR $\Delta F/F$ in response to
367 application of 10 mM glutamate was no different in WT and rd1 retinas, ruling out the possibility of impaired iGluSnFR
368 expression in rd1 retina (Fig. 5G). Taken together, these results suggest that reduced synaptic efficacy in degenerated
369 retina is caused by reduced evoked glutamate release from ON-BCs.

370

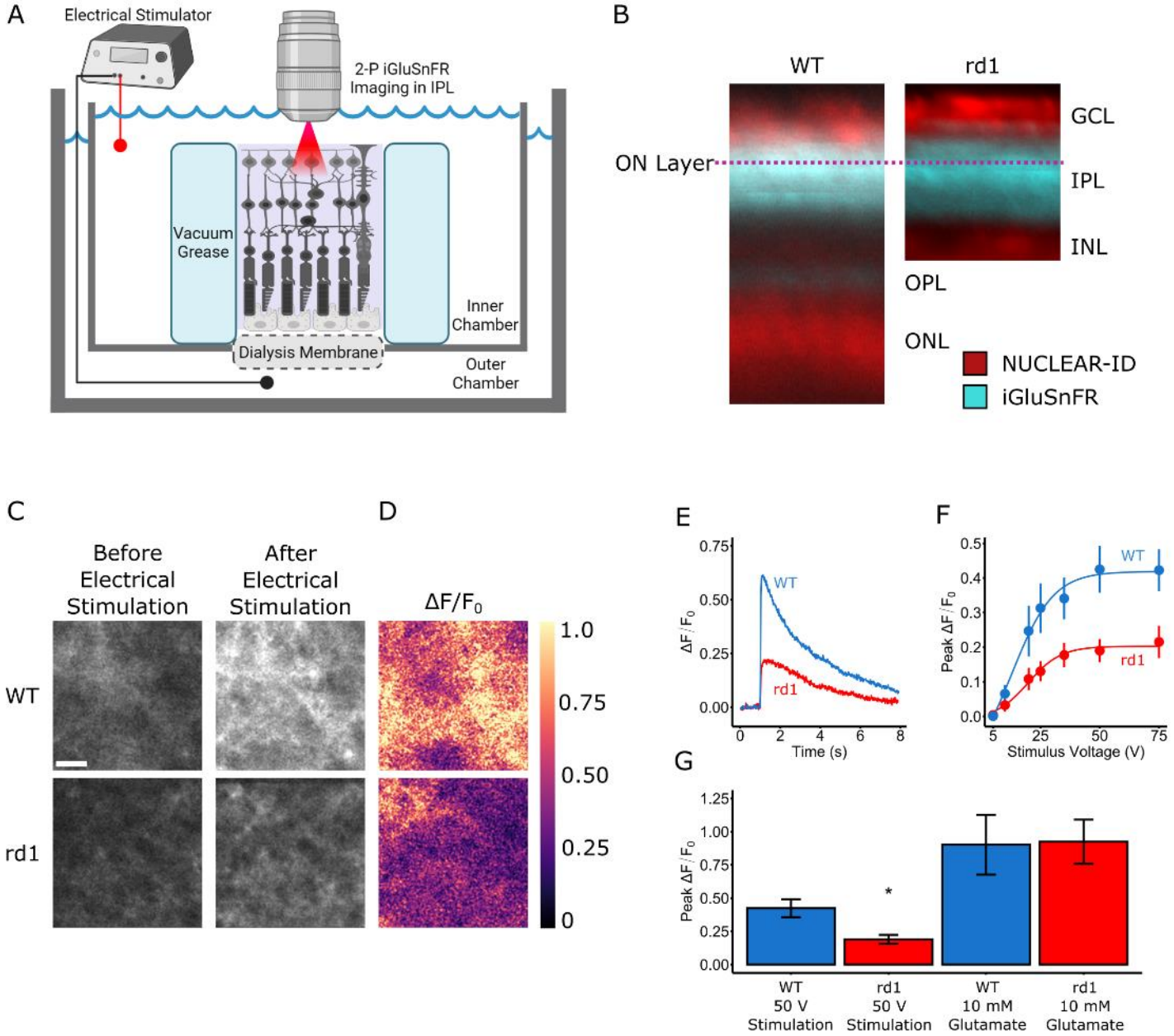

Figure 5. Synaptic release of glutamate from ON-BCs is reduced in retinas with photoreceptor degeneration. A) Apparatus for simultaneous trans-retinal electrical stimulation and 2-photon imaging of glutamate, the BC neurotransmitter. B) Virtual cross-sections (z-stacks) of retinas imaged with 2-photon microscopy. The genetically encoded fluorescent glutamate indicator iGluSnFR (cyan) was virally expressed throughout the IPL of WT) and rd1 retinas. The dashed line represents the ON Layer imaging plane, 10 µm into the IPL from the GCL border. Cell body layers were counterstained with a DNA-binding dye (NUCLEAR-ID, red). C) An optical section within the ON layer of the IPL before and 15 ms after stimulation, consisting of a 50 V, 2.5 ms shock in WT and rd1. D) The change in iGluSnFr fluorescence over background (ΔF/F), proportional to the change in glutamate concentration. Note that the fluorescence change upon stimulation is smaller in rd1 than in WT. E) Time course of the fluorescence change elicited by a single 2.5 ms, 50 V shock in a WT and rd1 retina. F) Peak iGluSnFR ΔF/F in response to varying shock strength. G) Peak iGluSnFR ΔF/F in response to a saturating 50 V, 2.5 ms shock is lower in rd1 than in WT ($p = 0.02$, $N = 7$ retinas). Peak iGluSnFR ΔF/F in response to application of 10 mM glutamate is no different between WT and rd1 retinas ($p = 0.71$, $N = 7$ retinas). Barplots indicate median value; error bars indicate ± SEM. Scale bar: 5 µm. All statistical comparisons were made with PWT with FDR correction.

387 **Retinoic acid mediates physiological remodeling of BCs**

388 RA triggers physiological remodeling of RGCs in the degenerated retina. To explore whether RA also underlies
389 physiological remodeling of BCs we injected the eye with BMS 493, an inhibitor of the RA receptor, RAR (Germain et al.,
390 2009). Because the effects of RA are mediated by changes in gene expression that require days to take effect, BMS 493
391 treatment was given 5-7 days before functional analysis. First, we used patch clamp recording to measure voltage-gated
392 Ca^{2+} current from BCs in retinal slices (Fig. 6A). BMS 493 increased the Ca^{2+} current by up to 3-fold in both CBC6 cells
393 from rd1 mice and in RBCs from rd10 mice, approximating the Ca^{2+} current observed in BCs from WT retinas (Fig. 6B–E).
394 In contrast to rd1 CBC6 cells, Ca^{2+} current in WT CBC6 cells was unaffected by BMS 493 (Fig. 6F–G). These findings
395 suggest that elevated RA decreases the Ca^{2+} conductance and that blocking RA signaling restores the conductance, by
396 changing the number of active Ca^{2+} channels, or altering their functional properties. Steady-state I vs. V curves show
397 that BMS 493 caused no shift in voltage-dependent activation (Fig. 6C,E,G), suggesting that RA caused no change in
398 gating of the Ca^{2+} channels.

399 Next, we examined the effect of inhibiting RA signaling on the synaptic output of BCs (Fig. 6H). BMS 493 increased
400 optogenetically-elicited synaptic transmission from CBC6 cells by up to 35% in rd1 retina and 45% in rd10 retina (Fig. 6I),
401 nearly completely reversing the remodeling deficit (see Fig. 2C). BMS 493 also increased synaptic transmission from
402 RBCs, by up to 30% in rd1 retina and 50% in rd10 retina (Fig. 6J), again reducing the remodeling deficit (see Fig. 2I).

403 We observed that short-term synaptic plasticity is also altered in degenerated retinas. In WT retinas, the CBC6 output
404 synapse exhibits profound paired-pulse depression, in which the first optogenetic EPSC is much larger than the second.
405 This is consistent with WT BCs having a large Ca^{2+} current that depletes the readily-releasable pool of synaptic vesicles,
406 leaving few available to be released by a second stimulus (Fig. 6K,L) (Gomis et al., 1999; Singer and Diamond, 2006). In
407 contrast, paired-pulse depression is absent from rd1 or rd10 retinas, replaced in CBC6 synapses with paired-pulse
408 facilitation, where the second response is larger than the first (Fig. 6K,L). The absence of synaptic depression can be
409 explained by BCs in degenerated retina having a smaller Ca^{2+} current, which evokes little release during the first
410 stimulus, preserving more vesicles to be released during a second one. The emergence of synaptic facilitation is
411 consistent with previous results showing that reducing the size of intracellular Ca^{2+} transients in cone bipolar cells, either
412 by reducing extracellular Ca^{2+} concentration (Borst et al., 1995) or by increasing intracellular Ca^{2+} buffer (von Gersdorff
413 and Matthews, 1997) converts paired-pulse depression to paired-pulse facilitation.

414 We next asked whether the short-term plasticity profile observed in degenerated retinas could be reversed by inhibiting
415 RA signaling. Treatment with BMS 493 converted the CBC6 output synapse in rd1 retinas from facilitating to depressing,
416 similar to WT (Fig. 6K,L). Injecting all-trans RA (ATRA) into WT eyes reduced the amplitude of optogenetically-evoked
417 EPSCs and reduced paired-pulse depression, suggesting that RA signaling is sufficient to trigger changes in the BC output
418 synapse (Fig. 6K,L). These findings implicate RA as the key signal that alters short-term plasticity of the BC output
419 synapse as a consequence of degeneration.

420 We further explored short-term plasticity by systematically changing the interstimulus interval. The CBC6 output
421 synapse in WT retinas exhibited paired-pulse depression across a wide range of intervals (Fig. 6M). However, in rd1
422 retinas, the synapse exhibited facilitation at short interstimulus intervals, but depression at longer intervals. The
423 involvement of multiple Ca^{2+}-dependent events occurring at different subcellular locations could explain this shift in
424 short term plasticity. With a smaller Ca^{2+} current, intracellular Ca^{2+} will rise more slowly and be more tightly constrained
425 within a nanodomain near the plasma membrane (Zucker and Regehr, 2002), preferentially engaging different Ca^{2+}
426 sensors than a larger Ca^{2+} current. Different isoforms of synaptotagmin, each with a distinct Ca^{2+} affinity, underlie
427 different events in synaptic release (e.g. vesicle replenishment and fusion) (Bacaj et al., 2013; Jackman et al., 2016;
428 Weingarten et al., 2022) and these Ca^{2+} sensors will be differentially activated depending on the intracellular Ca^{2+} profile,
429 which is sensitive to the interval between individual Ca^{2+} transients.

430

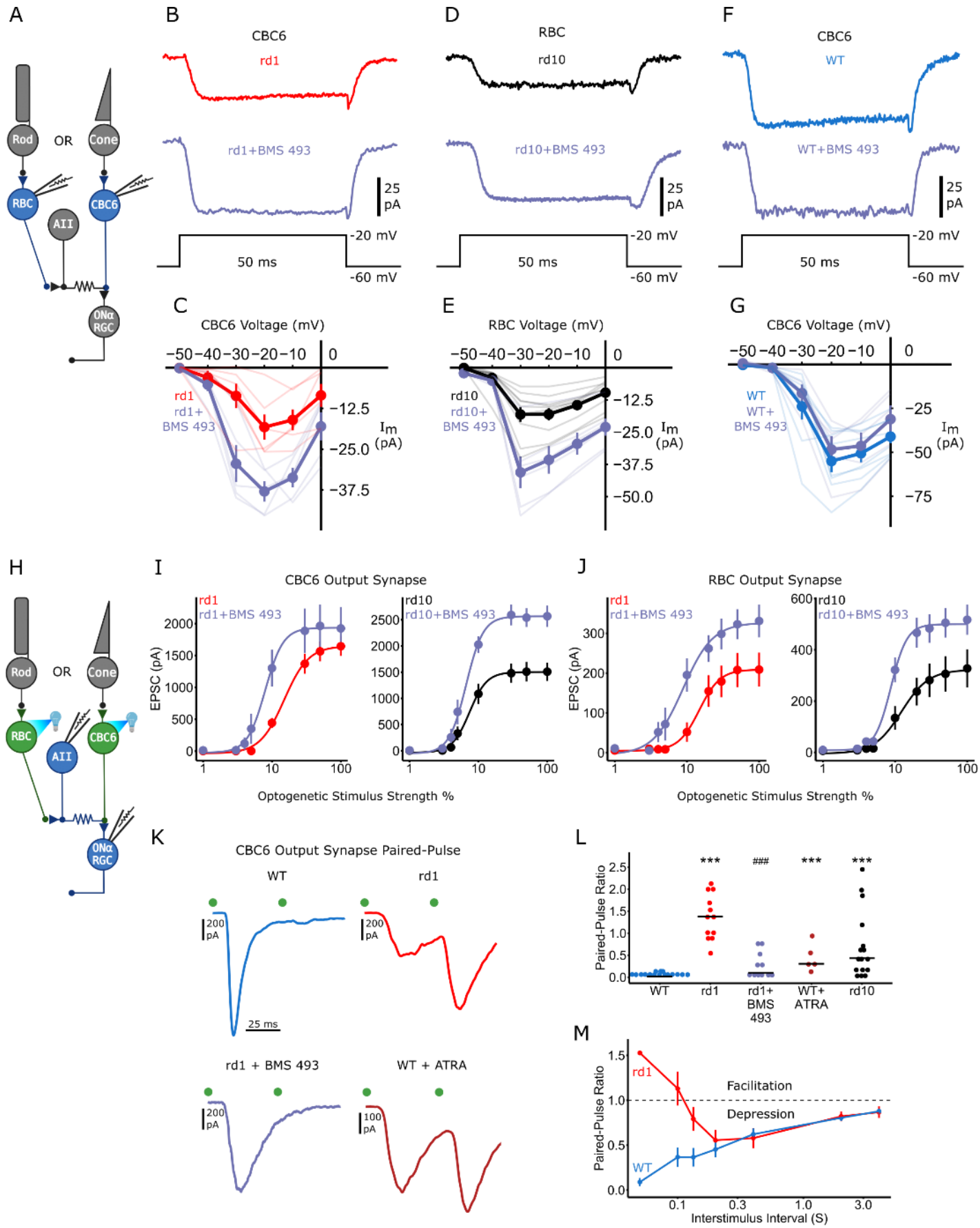
A
Rod
OR
Cone
RBC
AII
CBC6
ONα RGC
B
CBC6
rd1
rd1+BMS 493
25 pA
-20 mV
50 ms
-60 mV
D
RBC
rd10
rd10+BMS 493
F
CBC6
WT
WT+BMS 493
C
CBC6 Voltage (mV)
rd1
rd1+ BMS 493
Im (pA)
E
RBC Voltage (mV)
rd10
rd10+ BMS 493
G
CBC6 Voltage (mV)
WT
WT+ BMS 493
H
I
CBC6 Output Synapse
EPSC (pA)
Optogenetic Stimulus Strength %
J
RBC Output Synapse
K
CBC6 Output Synapse Paired-Pulse
WT
rd1
rd1 + BMS 493
WT + ATRA
25 ms
L
Paired-Pulse Ratio
WT
rd1
rd1+ BMS 493
WT+ ATRA
rd10
M
Facilitation
Depression
Interstimulus Interval (S)

431

Figure 6. RA signaling is necessary and sufficient for physiological remodeling of BCs. A) Retinal circuit diagram showing direct recording of calcium current from either CBC6 or RBC. B,D,F) Inward calcium currents in BCs treated with BMS 493 from rd1 CBC6, rd10 RBCs, and WT CBC6 respectively. Current was activated with a depolarizing voltage step (50 ms) from -60 mV to -20 mV. Steady-state current vs. voltage (I-V) curves, elicited with a series of 10 mV incrementing depolarizing steps from -60 mV. C,E,G) I-V curves show that the BMS 493 significantly rescues voltage-gated calcium current in both CBC6 cells in rd1 retina ($p < 0.001$) and RBCs in the rd10 retina ($p < 0.001$). CBC6 cells: rd1, N = 6; rd1 + BMS 493, N = 5. RBCs: rd10, N = 10, rd10 + BMS 493, N = 7. BMS 493 treatment had no effect on voltage-gated calcium current in WT CBC6 cells ($p = 0.93$). WT: N = 8; WT + BMS 493: N = 5.) BMS 493 treatment compared to dataset from Fig.1. H) Retinal circuit diagram showing optogenetic stimulation of either CBC6 cells or RBCs. I, J) EPSC magnitude vs. optogenetic stimulus strength. BMS 493 increased EPSC magnitude in ON α-RGCs in rd1 ($p=0.006$) and rd10 retinas ($p<0.001$). RGCs: rd1, N = 15; rd1 + BMS 493, N = 11; rd10, N = 11; rd10 + BMS 493, N = 8. H). BMS 493 also increased EPSC magnitude in AII amacrine cells in rd1 ($p=0.001$) and rd10 retinas ($p<0.001$). AII amacrine cells, rd1: N=10, rd1 + BMS 493: N=9, rd10: N=14, rd10 + BMS 493: N=12. BMS 493 treatment compared to dataset from Fig.2 K) EPSCs from ON α-RGCs in response to paired pulse flashes given with a 50 ms interval. Green dots indicate light flash. WT shows complete paired-pulse depression and rd1 shows no paired-pulse depression. Note that BMS 493 induces paired-pulse depression in rd1 and ATRA eliminates paired-pulse depression in WT. L) Quantification of the paired pulse ratio (EPSC 2 / EPSC 1) for the 50 ms interstimulus interval. Compared to WT, paired EPSCs exhibited less synaptic depression in rd1 ($p<0.001$), rd10 ($p=0.004$), and ATRA-treated WT retinas ($p<0.001$) denoted with ***. BMS 493 treatment increased synaptic depression in rd1 retinas ($p<0.001$) denoted with ###. WT: N=16, rd1: N=13, rd10: N=16, rd1 + BMS 493: N=11, WT + ATRA: N=5. Horizontal lines indicate median values: WT=0.02, rd1=1.38, rd10=0.43, rd1 + BMS 493=0.10, WT + ATRA=0.30. M) Paired-pulse ratio changes as a function of interstimulus interval. Paired-pulse optogenetic pulse width: 1 ms. Error bars indicate ± SEM. Transparent traces indicate individual cells. All statistical comparisons were made with PWT with FDR correction.

455 **Physiological remodeling of BCs alters spatiotemporal information processing.**

456 In the WT retina, sensory information from an array of photoreceptors signals through a series of retinal neurons,
457 ultimately converging onto an RGC to produce a classical receptive field. In a photoreceptor-degenerated retina with the
458 responses of a particular type of BC under optogenetic control, each RGC receives a projective field, reflecting the
459 convergence of information from that specific BC cell type. Here we compare rd1 and WT retinas to ask whether
460 photoreceptor degeneration alters the CBC6 to ON α-RGC projective field. We optogenetically stimulated small clusters
461 of CBC6 cells with 50 µm spots of light to yield a spatial map of BCs projecting onto an individual ON α-RGC (Fig. 7A–C).
462 We found that the spatial map in rd1 retinas is nearly identical to the map in WT retina, but scaled down linearly (Fig.
463 7D,E), presumably owing to decreased synaptic transmission. This finding is consistent with previous work showing little
464 change in cone-mediated RGC receptive field size following rod degeneration, in a different mouse model of RP
465 (Scalabrino et al., 2022).

466 We next compared the temporal properties of the CBC6 to ON α-RGC network in WT and photoreceptor degenerated
467 retinas. We optogenetically stimulated populations of CBC6 cells at different rates and recorded either EPSCs in whole-
468 cell patch recordings or spiking in cell-attached patch recordings from individual RGCs (Fig. 8A). In the WT retina, a low
469 frequency train of stimuli (0.25 Hz) evoked a non-decrementing train of EPSCs (Fig. 8B,G). Even with higher frequency
470 stimulation (up to 7.5 Hz), EPSCs followed reliably, although their amplitudes declined during the train (Fig. 8B,G–I). In
471 rd1 and rd10 retinas, EPSCs were non-decrementing at low frequency (0.25 Hz), but their amplitudes declined rapidly at
472 higher frequencies, with EPSCs failing completely by the end of the 7.5 Hz stimulation train. To confirm that optogenetic
473 stimulation caused reliable depolarizations that were equivalent in WT and rd10 retinas, we recorded from CBC6 cells
474 under current clamp while applying trains of light flashes. Except for a ~50% decline in amplitude between the first and
475 second depolarization, subsequent depolarizations showed little decrement for at least 3 s, when flashes were repeated
476 at 7.5 Hz (Fig. 8C,D). Hence changes in presynaptic depolarizations cannot account for the failure of postsynaptic
477 responses.

478 Comparing across all stimulation rates, the frequency at which EPSCs declined by 90% (-10 dB) at steady state was 5.25
479 Hz for WT, 0.68 Hz for rd1, and 2.47 Hz for rd10. (Fig. 8J). Despite this dramatic decline, an EPSC could still be evoked if a
480 greatly prolonged depolarizing stimulus were applied at the end of the train (Fig. 8E,F), suggesting that even though the
481 pool of readily-releasable vesicles had been depleted, it could be resupplied from a reserve pool, given a sufficiently
482 large and prolonged intracellular Ca^{2+} signal. Vesicle resupply is a Ca^{2+}-accelerated processes, involving an isoform of
483 synaptogamin distinct from the isoform that underlies vesicle fusion (Weingarten et al., 2022) and perhaps the large Ca^{2+}
484 signal engages this process.

485 Decrementing synaptic efficacy would be expected to adversely impact action potential reliability in RGCs. To test this,
486 we made cell-attached patch-clamp recordings to non-invasively monitor spike activity from ON α-RGCs. In the WT
487 retina, RGC firing followed optogenetic BC stimulation reliably up to 7.5 Hz (Fig. 8K), consistent with temporal tuning of

488 normal light responses in ON α-RGCs in WT retinas (Tien et al., 2017). In the rd1 and rd10 retina, firing failed to follow
489 even at 2.5 Hz stimulation frequency. We compiled firing reliability data over a wide range of stimulus frequencies and
490 train durations. RGCs failed to follow BC stimulation at a low frequency in rd10 and an even lower frequency in rd1 (Fig.
491 8L). The decline of reliability in the CBC6 to ON α-RGC network can be attributed entirely to changes in the BCs. We
492 found no difference in the frequency response of ON α-RGC to firing induced by direct current injection in WT and
493 degenerated retinas (data not shown). These findings illustrate the severe deficit that BC physiological remodeling
494 imposes on information transfer to RGCs in the degenerated retina.

495 Equivalent experiments on RBC output synapse showed an even more extreme frequency-dependent decline in
496 photoreceptor degenerated retina (Fig. 9A,B). Even at 0.25 Hz, EPSCs from rd1 and rd10 retinas began decrementing
497 while WT did not (Fig. 9B,C). Higher stimulation frequency led to the near complete loss of EPSCS in rd1 and rd10 at
498 steady state (Fig. 9B,E–G). Current clamp recordings from RBCs confirmed that optogenetic stimulation caused reliable
499 depolarizations that were equivalent in WT and rd10 retinas (Fig. 9C,D). Hence as was the case for CBC6 cells, changes
500 in presynaptic depolarizations in RBCs cannot account for the failure of postsynaptic responses.

501 Comparing all stimulation rates, the frequency at which EPSCs declined by 90% (-10 dB) at steady state was 5.14 Hz for
502 WT, 0.69 Hz for rd1, and 1.34 Hz for rd10. (Fig. 9H). Since the vast majority of ON BC types receive direct or indirect
503 input from RBCs, the decrementing responses in photoreceptor degenerated retinas is expected to adversely impact a
504 wide variety of ON-RGCs beyond just the ON α-RGC subtype.

505

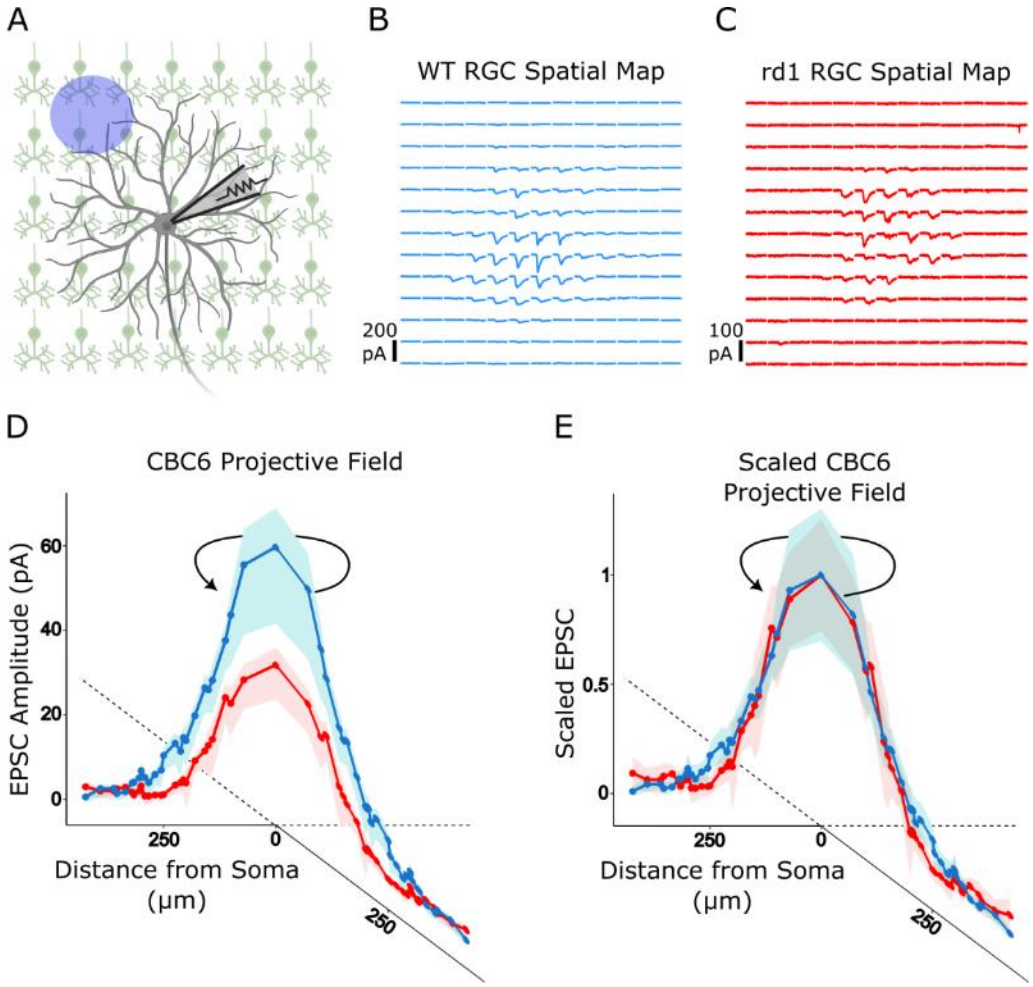

506

507 **Figure 7. The spatial map of the BC to RGC network is preserved in photoreceptor degenerated retina but scaled down**
508 **linearly.** A) Schematic diagram of the experiment. To map the projective field corresponding to many CBC6 cells
509 converging onto a single ON α-RGC, we used 50 µm non-overlapping spots of light to optogenetically stimulate clusters
510 of BCs, covering the entire dendritic tree of the ON α-RGCs. B-C) Example spatial projective field map from a WT (B) and
511 rd1 (C) retina. Detectable EPSCs were elicited over ~200 μm^2 of the 650 μm^2 mapped area. D) Group data from ON α-
512 RGCs (N=9 each), with the projective field represented as mean EPSC vs. distance from the cell soma. Data from all
513 directions from the cell center were averaged and are shown duplicated for clarity. Note that EPSCs were smaller in rd1
514 than WT (p=0.012), but there was no difference in spatial weighting of the linearly scaled projection field (p=0.47).
515 Variability ribbons indicate 95% confidence intervals. All statistical comparisons were made with PWT with FDR
516 correction.

517

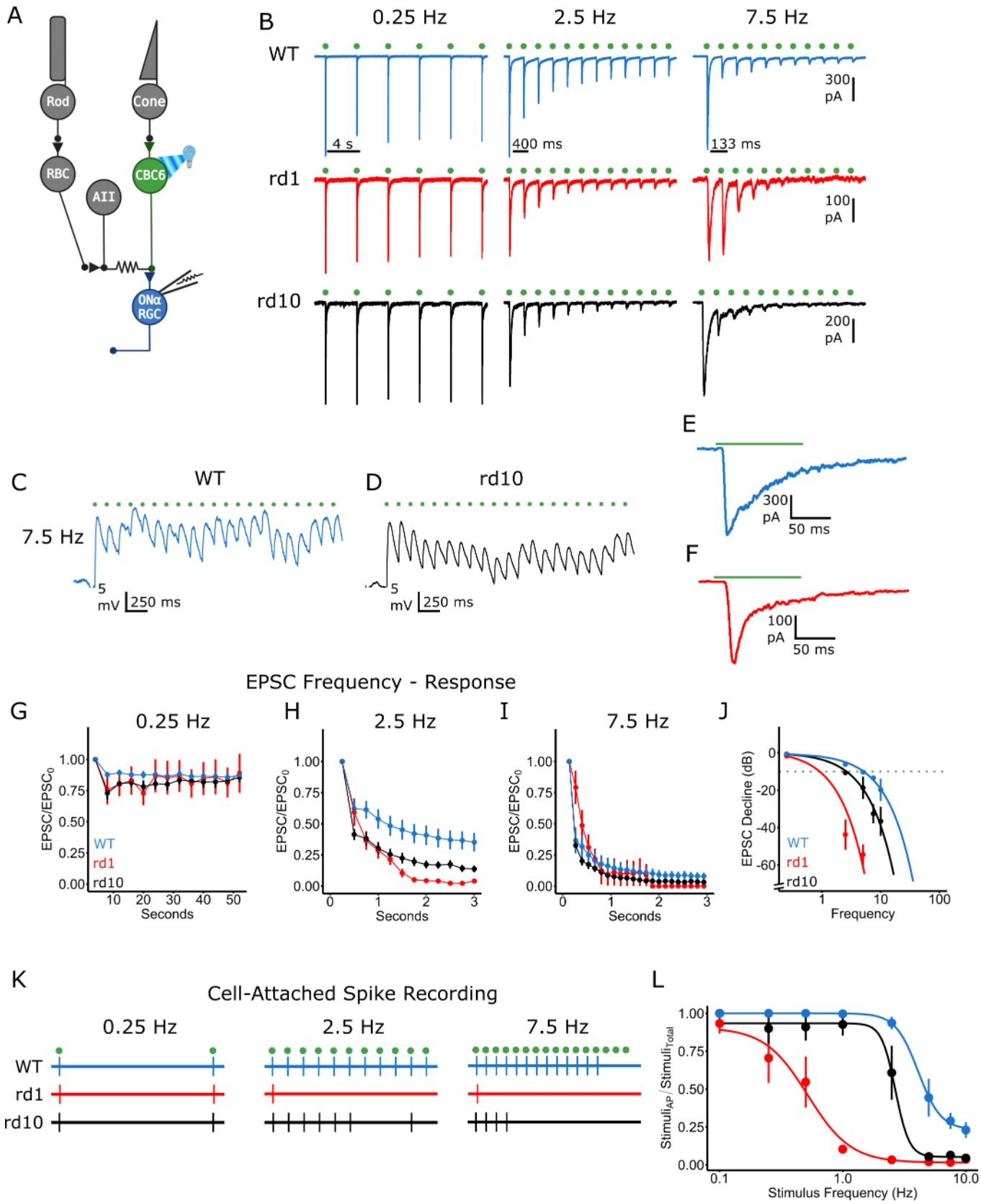
A
Rod
Cone
RBC
AII
CBC6
ONα RGC
B
0.25 Hz
2.5 Hz
7.5 Hz
WT
rd1
rd10
4 s
400 ms
133 ms
300 pA
100 pA
200 pA
C
WT
7.5 Hz
5 mV
250 ms
D
rd10
5 mV
250 ms
E
300 pA
50 ms
F
100 pA
50 ms
EPSC Frequency - Response
G
0.25 Hz
H
2.5 Hz
I
7.5 Hz
J
EPSC/EPSC0
Seconds
WT
rd1
rd10
EPSC Decline (dB)
Frequency
K
Cell-Attached Spike Recording
0.25 Hz
2.5 Hz
7.5 Hz
WT
rd1
rd10
L
Stimuli_AP / Stimuli_Total
Stimulus Frequency (Hz)

518

519

520

Figure 8. Photoreceptor degeneration reduces the frequency response in the cone pathway. A) CBC6 cells were optogenetically stimulated at different rates while EPSCs were recorded in an ON α-RGC. B) EPSCs elicited by stimuli repeated at 0.25 Hz, 2.5 Hz, and 7.5 Hz. Green dots indicate the time of light flash: 2.5 ms pulse width. C, D) Recording membrane voltage directly in CBC6 from WT and rd10 little decrement in depolarization following 7.5 Hz optogenetic stimulation. E, F) Immediately following a 5 Hz optogenetic stimulation train, a 100 ms pulse was given resulting in a large EPSC despite a depressed synapse in both a WT and rd1. G – I) EPSCs in rd1 and rd10 retinas diminish faster with increasing stimulation frequency. J) EPSC decline expressed in dB ($10Log\frac{EPSC_{Final}}{EPSC_{Initial}}$) for each stimulation frequency. The continuous line is the fit with a linear function. (WT: N=7, $y = -0.143 - 1.93x$, R^2= 1.00; rd1: N = 9, $y = 1.42 - 12.5x$, R^2= 0.99,; rd10: N=10 $y = 0.272 - 3.93x$, R^2= 0.95). The dotted line is $y = -10\ dB$. EPSCs for rd1 at 7.5 and 10 Hz become immeasurably small at steady state. K) Raster of cell-attached spike recordings from stimulation at 0.25 Hz, 2.5 Hz, and 7.5 Hz. Green dots indicate light flash. L) The ratio of stimuli that produced an action potential to the total number of stimuli per frequency. Compared to WT, rd1 and rd10 ON α-RGCs successfully encoded fewer stimuli as stimulation frequency increased. WT: N=6, rd1, N=6, rd10, N = 5 cells.(rd1: $p<0.001$, rd10: $p=0.034$. PWT with FDR correction). Error bars indicate ± SEM.

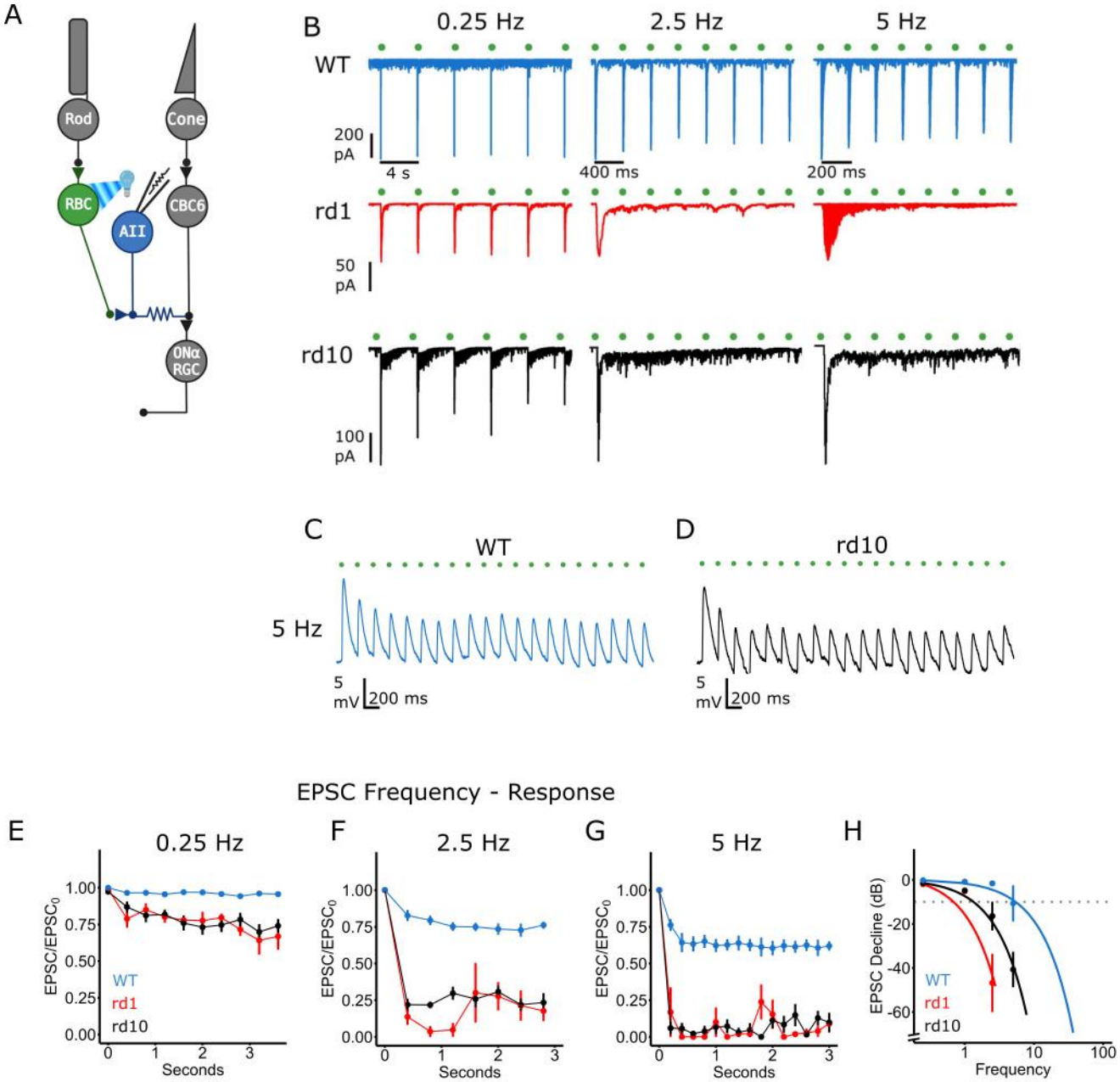

Figure 9. Photoreceptor degeneration reduces the frequency response in the rod pathway. A) RBCs cells were optogenetically stimulated at different rates while EPSCs were recorded in an AII amacrine cell. B) EPSCs elicited by stimuli repeated at 0.25 Hz, 2.5 Hz, and 5 Hz. Green dots indicate the time of light flash: 5 ms pulse width. C, D) Recording membrane voltage directly in RBCs from WT and rd10 little decrement in depolarization following 5 Hz optogenetic stimulation. E–G) EPSCs in rd1 and rd10 retinas diminish faster with increasing stimulation frequency. H) EPSC decline expressed in dB ($10Log\frac{EPSC_{Final}}{EPSC_{Initial}}$) for each stimulation frequency. The continuous line is the fit with a linear function. (WT: N=6, $y = -0.28 - 1.89x$, R^2= 0.90; rd1: N=5, $y = 2.63 - 18.4x$, R^2= 0.99,; rd10: N=11, $y = 0.579 - 7.91x$, R^2= 0.94). The dotted line is $y = -10\ dB$. EPSCs for rd1 at 5 Hz become immeasurably small at steady state. Error bars indicate ± SEM.

547 **Discussion**

548 This paper reports the surprising finding that photoreceptor degeneration leads to dramatic functional weakening of the
549 output synapses of ON-BCs. RBCs, the most numerous type of BC in the rod-dominant mouse retina, and CBC6 cells,
550 which receive information from both rod and cone pathways, are both affected. The net effect of these changes in BCs
551 is to reduce the amplitude and narrow the frequency response of light onset signals sent to RGCs and onward to the
552 brain. Our imaging results with iGluSnFr suggests that glutamate release from OFF-BCs might also be reduced in the
553 degenerated retina, which might also reduce signals at light offset. New cell-type selective promoters for particular OFF-
554 BCs could help address this point.

555 Previous experiments on a rat model of RP showed that ON-RGCs exhibit reduced spontaneous firing, paralleling the loss
556 of the RGC light response (Sekirnjak et al., 2011). The most obvious explanation for the decline in spontaneous and
557 evoked ON-RGC activity is that the diminishing number of photoreceptors drives a declining amount of excitatory
558 synaptic input. However, the possibility that changes intrinsic to ON-BCs also contributed to changes in ON-RGC activity
559 remained unexplored. Our discovery that the output synapse of ON-BCs is dramatically weakened adds an important
560 new mechanism that may contribute to changes in ON-RGC activity across species, not only corrupting retinal signal
561 processing, but also contributing to the pathophysiology of vision loss.

562 Another consequence of photoreceptor loss is the emergence of membrane potential oscillations in the inner retina,
563 ultimately resulting in spontaneous burst firing in RGCs (Trenholm and Awatramani, 2015). The oscillation is initiated in
564 the electrically coupled network of AII amacrine cells (Choi et al., 2014), but it remains to be determined if RA-mediated
565 events are involved.

566 **Mechanism of physiological remodeling**

567 Our findings suggest that RA is necessary and sufficient for physiological remodeling of the ON-BC output synapse.
568 Adding exogenous ATRA mimics changes in synaptic release that are characteristic of degenerated retinas (Fig. 6K).
569 Inhibiting RAR with BMS 493 reverses changes in synaptic release and restores voltage-gated Ca^{2+} current to near WT
570 levels (Fig. 6). Our previous studies utilizing an RA-induced reporter demonstrated elevated RA-induced gene expression
571 in degenerated retina (Telias et al., 2019).

572 It remains unclear where the excessive RA is produced. RA has been implicated in physiological remodeling not only in
573 the output synapses of BCs but also in RGCs (Telias et al., 2019). Moreover, RA is critical for morphological remodeling of
574 BC dendrites, at their input synapses (Lin et al., 2012). The fact that multiple cell types are affected in a degenerated
575 retina suggests that RA might act in a paracrine fashion, produced by one cell type (perhaps RPE cells), and diffusing
576 throughout the retina to trigger remodeling in many cell types. Immunocytochemistry and enzyme assays show that the
577 retina, choroid, and RPE all express isoforms of RALDH, the enzyme that synthesizes RA (Harper et al., 2015). In the RPE,
578 RALDH normally converts all-trans retinaldehyde released from photobleached rhodopsin into RA (McCaffery et al.,

579 1996). The loss of photoreceptors might increase the concentration of retinaldehyde, leading to increased production of
580 RA by the RPE. In this scenario, RA would be an intercellular signal, diffusing from the outer to the inner retina to exert
581 its actions. Alternatively, it is possible that RA is synthesized within particular retinal neurons and serves as an
582 intracellular messenger. In neurons in the hippocampus, local production of RA in dendrites regulates local gene
583 translation, a key event underlying homeostatic synaptic plasticity (Thapliyal et al., 2022) .

584 How does elevated RA decrease voltage-gated Ca^{2+} current and synaptic transmission? The size of the Ca^{2+} current in
585 ON-BCs is reduced by photoreceptor degeneration, but the activation and inactivation properties are unchanged,
586 suggesting a decreased level of channel protein rather than a change in channel type. RAR is an enhancer of gene
587 transcription, which often results in increased expression of specific proteins. However, there are many examples of RA-
588 induced down-regulation of proteins, mediated by a sign-inverting gene regulatory cascade (Balmer and Blomhoff,
589 2002).

590 L-type Ca^{2+} channels are complexed with accessory proteins, including alpha-2/delta subunits that determine Ca^{2+}
591 current density and activation/inactivation kinetics (Dolphin, 2009), in addition to controlling vesicle release probability
592 at synapses (Hoppa et al., 2012). It is possible that functional down-regulation of Ca^{2+} channels is caused by
593 misregulation of alpha-2/delta, as occurs in sensory neurons in dorsal root ganglia after nerve injury (D'Arco et al.,
594 2015). Transcriptomic analysis of BCs indicates that there are changes in gene expression, but they are limited to only a
595 few genes(Gilhooley et al., 2021), which could simplify the task of identifying the molecular basis of calcium current
596 down-regulation. Many other RA-induced biochemical events could also result in decreased Ca^{2+} current, including
597 altered post-translational modification or altered membrane trafficking of Ca^{2+} channel proteins (D'Arco et al., 2015).

598 Is the loss of Ca^{2+} channels sufficient to account for the decline in synaptic release, without invoking additional changes
599 in the release machinery? We find no decline in the number of synaptic contacts between BCs and RGCs and no loss of
600 synaptic ribbons, a key component of the BC synaptic machinery. Hence, at least at this age (p60) in rd1 mice,
601 photoreceptor degeneration causes no obvious structural changes in the BC output synapse. We did observe one
602 interesting phenomenon concerning the frequency-dependence of the ON-BC output synapse in the degenerated retina,
603 but it also may be explained by decreased Ca^{2+} influx during stimulation. We found that paired-pulse depression was
604 dramatically decreased in rd1 and rd10 retinas (Fig. 6K), whereas there was a great increase in failure of the synapse
605 with more sustained, high-frequency stimulation (Fig. 8J). Intracellular Ca^{2+} regulates synaptic vesicle fusion to the
606 plasma membrane, but it is also thought to regulate other steps in the synaptic vesicle cycle, such as vesicle docking and
607 priming (Wan and Heidelberger, 2011). In fact, there is evidence for multiple Ca^{2+}-dependent steps in the vesicle cycle at
608 BC ribbon synapses (Gomis et al., 1999). If Ca^{2+} influx were sufficient to cause vesicle fusion but insufficient to accelerate
609 vesicle resupply, repetitive stimulation might deplete the pool of readily releasable vesicles before they could be
610 replenished. Different isoforms of synaptotagmin mediate fusion and resupply (Weingarten et al., 2022), providing

611 opportunities for understanding how reduced Ca^{2+} influx in remodeled BCs affects synaptic transmission at the
612 molecular level.

613 **Functional impact**

614 Our results imply that physiological remodeling of ON-BCs will constrain information processing further along in the
615 visual system, limiting visual perception. The deficit in temporal coding caused by decreased ON-BC output was
616 particularly severe, which is expected to have a particularly large impact on perception of object motion. Humans with
617 RP often fail to detect moving objects or report motion in the opposite direction of actual movement (Turano and Wang,
618 1992), even if they retain significant visual acuity for detecting static objects (Alexander et al., 1998). RP is a progressive
619 disease that causes gradual vision loss, but the distinct contributions of decreased photoreceptor density vs.
620 physiological remodeling to vision decline is unclear. Our previous results (Telias et al., 2022) showed that treatments
621 that reverse physiological remodeling could substantially rescue visual contrast sensitivity in rd10 mice at 2-3 months of
622 age, when photoreceptor degeneration is already severe. We now know that physiological remodeling applies not only
623 to RGCs, but also to BCs, but whether remodeling of one cell type or the other predominates in altering visual
624 perception is also unknown.

625 In certain respects, the physiological remodeling that we characterized in ON-BCs might be considered a homeostatic
626 mechanism, analogous to other compensatory events caused by partial photoreceptor loss (Lee et al., 2022). In the
627 healthy retina, photoreceptors tonically release glutamate, which keeps ON-BCs hyperpolarized. Hypothetically, by
628 eliminating glutamate release, photoreceptor death should depolarize the ON-BCs, chronically activating their voltage-
629 gated Ca^{2+} channels, and increasing their tonic release of glutamate onto RGCs. If this chronic synaptic excitation of RGCs
630 were sufficient to trigger firing, it could impair encoding of synaptic information from other BCs that had yet to undergo
631 remodeling. One way that ON-BCs could compensate for excessive depolarization is by down-regulating their Ca^{2+}
632 channels. While the loss of Ca^{2+} channels might be adaptive, by preventing excessive output from ON-BCs, it comes at a
633 cost. We have demonstrated that physiological remodeling limits the dynamic range of the synaptic output of CBC6 cells
634 (Fig. 2C) and RBCs (Fig. 2I) and severely limits temporal reliability (Fig. 7,8), which is maladaptive for encoding visual
635 information. The degree of photoreceptor loss may determine whether physiological remodeling is adaptive or
636 maladaptive.

637 Our findings that physiological remodeling of ON-BCs, as well as RGCs, can be reversed by inhibiting RA has important
638 implications for preserving sight in low-vision patients with RP and perhaps other photoreceptor degenerative disorders.
639 They also have important implications for vision restoration in advanced RP patients with nearly complete
640 photoreceptor loss and little remaining light perception. One treatment approach for these patients is to install light
641 responses in surviving neurons of the outer retina, including ON-BCs, either through optogenetic stimulation (Lagali et
642 al., 2008; Sahel et al., 2021) or electrical stimulation with sub-retinal implants (Roux et al., 2016). While ON-BCs in
643 mouse models of RP do retain the ability to transmit optogenetically-elicited synaptic signals to RGCs (Lagali et al.,

644 2008), our findings suggest that physiological remodeling of the ON-BC output synapse will limit downstream
645 information processing and visual perception. Our results indicate that reduced frequency-response of the ON-BC
646 output synapse, seen as a failure of EPSCs, severely impairs RGC spike-rate coding. In the clinical context, this may
647 severely limit the effectiveness of optogenetic therapies targeted to ON-BCs or upstream remnant photoreceptors in
648 degenerated retina. The same problems may also apply to signals initiated by stem-cell derived regenerated
649 photoreceptors inserted into the outer retina. Inhibiting RA synthesis or signaling may remove these problems and
650 augment the effectiveness of any vision restoration technology that delivers light-elicited signals to the blind retina. RA
651 inhibition can be accomplished with pharmacological inhibitors of RALDH or RAR (Telias et al., 2022), or with targeted
652 AAV vectors that deliver genetic-based inhibitors of RALDH and RAR to specific retinal cell types, for example ON-BCs or
653 RGCs (Bi et al., 2006; Lagali et al., 2008).

654

655 References

656 Alexander KR, Derlacki DJ, Xie W, Fishman GA, Szlyk JP (1998) Discrimination of spatial displacements by patients with
657 retinitis pigmentosa. Vision Res 38:1171–1181.

658 Bacaj T, Wu D, Yang X, Morishita W, Zhou P, Xu W, Malenka RC, Südhof TC (2013) Synaptotagmin-1 and synaptotagmin-7
659 trigger synchronous and asynchronous phases of neurotransmitter release. Neuron 80:947–959.

660 Balmer JE, Blomhoff R (2002) Gene expression regulation by retinoic acid. J Lipid Res 43:1773–1808.

661 Behrens C, Yadav SC, Korympidou MM, Zhang Y, Haverkamp S, Irsen S, Schaedler A, Lu X, Liu Z, Lause J, St-Pierre F,
662 Franke K, Vlasits A, Dedek K, Smith RG, Euler T, Berens P, Schubert T (2022) Retinal horizontal cells use different
663 synaptic sites for global feedforward and local feedback signaling. Curr Biol 32:545-558.e5.

664 Bi A, Cui J, Ma Y-P, Olshevskaya E, Pu M, Dizhoor AM, Pan Z-H (2006) Ectopic Expression of a Microbial-Type Rhodopsin
665 Restores Visual Responses in Mice with Photoreceptor Degeneration. Neuron 50:23–33.

666 Borst JG, Helmchen F, Sakmann B (1995) Pre- and postsynaptic whole-cell recordings in the medial nucleus of the
667 trapezoid body of the rat. J Physiol 489:825–840.

668 Care RA, Kastner DB, De la Huerta I, Pan S, Khoche A, Santina LD, Gamlin C, Tomas CS, Ngo J, Chen A, Kuo Y-M, Ou Y,
669 Dunn FA (2019) Partial Cone Loss Triggers Synapse-Specific Remodeling and Spatial Receptive Field
670 Rearrangements in a Mature Retinal Circuit. Cell Rep 27:2171-2183.e5.

671 Choi H, Zhang L, Cembrowski MS, Sabottke CF, Markowitz AL, Butts DA, Kath WL, Singer JH, Riecke H (2014) Intrinsic
672 bursting of AII amacrine cells underlies oscillations in the rd1 mouse retina. J Neurophysiol 112:1491–1504.

673 Dalkara D, Byrne LC, Klimczak RR, Visel M, Yin L, Merigan WH, Flannery JG, Schaffer DV (2013) In vivo-directed evolution
674 of a new adeno-associated virus for therapeutic outer retinal gene delivery from the vitreous. Sci Transl Med
675 5:189ra76.

676 D'Arco M, Margas W, Cassidy JS, Dolphin AC (2015) The Upregulation of α2δ-1 Subunit Modulates Activity-Dependent
677 Ca2+ Signals in Sensory Neurons. J Neurosci 35:5891–5903.

678 Dolphin AC (2009) Calcium channel diversity: multiple roles of calcium channel subunits. Curr Opin Neurobiol 19:237–
679 244.

680 Dunn FA (2015) Photoreceptor Ablation Initiates the Immediate Loss of Glutamate Receptors in Postsynaptic Bipolar
681 Cells in Retina. J Neurosci 35:2423–2431.

682 Ellis EM, Paniagua AE, Scalabrino ML, Thapa M, Rathinavelu J, Jiao Y, Williams DS, Field GD, Fain GL, Sampath AP (2023)
683 Cones And Cone Pathways Remain Functional in Advanced Retinal Degeneration. Curr Biol 33:1513-1522.e4.

684 Gayet-Primo J, Puthussery T (2015) Alterations in Kainate Receptor and TRPM1 Localization in Bipolar Cells after Retinal
685 Photoreceptor Degeneration. Front Cell Neurosci 9:486.

686 Germain P, Gaudon C, Pogenberg V, Sanglier S, Van Dorsselaer A, Royer CA, Lazar MA, Bourguet W, Gronemeyer H
687 (2009) Differential action on coregulator interaction defines inverse retinoid agonists and neutral antagonists.
688 Chem Biol 16:479–489.

689 Gilhooley MJ, Hickey DG, Lindner M, Palumaa T, Hughes S, Peirson SN, MacLaren RE, Hankins MW (2021) ON-bipolar cell
690 gene expression during retinal degeneration: Implications for optogenetic visual restoration. Exp Eye Res
691 207:108553.

692 Gomis A, Burrone J, Lagnado L (1999) Two Actions of Calcium Regulate the Supply of Releasable Vesicles at the Ribbon
693 Synapse of Retinal Bipolar Cells. J Neurosci 19:6309–6317.

694 Harper AR, Wiechmann AF, Moiseyev G, Ma J-X, Summers JA (2015) Identification of Active Retinaldehyde
695 Dehydrogenase Isoforms in the Postnatal Human Eye. PLoS One 10:e0122008.

696 Heidelberger R, Matthews G (1992) Calcium influx and calcium current in single synaptic terminals of goldfish retinal
697 bipolar neurons. J Physiol 447:235–256.

698 Helmstaedter M, Briggman KL, Turaga SC, Jain V, Seung HS, Denk W (2013) Connectomic reconstruction of the inner
699 plexiform layer in the mouse retina. Nature 500:168–174.

700 Hoppa MB, Lana B, Margas W, Dolphin AC, Ryan TA (2012) alpha2delta expression sets presynaptic calcium channel
701 abundance and release probability. Nature 486:122–125.

702 Humayun MS, Dorn JD, Cruz L da, Dagnelie G, Sahel J-A, Stanga PE, Cideciyan AV, Duncan JL, Eliott D, Filley E, Ho AC,
703 Santos A, Safran AB, Arditi A, Del Priore LV, Greenberg RJ (2012) Interim Results from the International Trial of
704 Second Sight's Visual Prosthesis. Ophthalmology 119:779–788.

705 Jackman SL, Turecek J, Belinsky JE, Regehr WG (2016) The calcium sensor synaptotagmin 7 is required for synaptic
706 facilitation. Nature 529:88–91.

707 Lagali PS, Balya D, Awatramani GB, Münch TA, Kim DS, Busskamp V, Cepko CL, Roska B (2008) Light-activated channels
708 targeted to ON bipolar cells restore visual function in retinal degeneration. Nature Neuroscience 11:667–675.

709 Lee JY, Care RA, Kastner DB, Santina LD, Dunn FA (2022) Inhibition, but not excitation, recovers from partial cone loss
710 with greater spatiotemporal integration, synapse density, and frequency. Cell Rep 38:110317.

711 Liang C-Q, Zhang G, Zhang L, Chen S-Y, Wang J-N, Zhang T-T, Singer JH, Ke J-B (2021) Calmodulin Bidirectionally Regulates
712 Evoked and Spontaneous Neurotransmitter Release at Retinal Ribbon Synapses. eNeuro 8:ENEURO.0257-
713 20.2020.

714 Lin Y, Jones BW, Liu A, Tucker JF, Rapp K, Luo L, Baehr W, Bernstein PS, Watt CB, Yang J-H, Shaw MV, Marc RE (2012)
715 Retinoid receptors trigger neuritogenesis in retinal degenerations. FASEB J 26:81–92.

716 Marc RE, Jones BW, Watt CB, Strettoi E (2003) Neural remodeling in retinal degeneration. Progress in Retinal and Eye
717 Research 22:607–655.

718 Mazzoni F, Novelli E, Strettoi E (2008) Retinal Ganglion Cells Survive and Maintain Normal Dendritic Morphology in a
719 Mouse Model of Inherited Photoreceptor Degeneration. J Neurosci 28:14282–14292.

720 McCaffery P, Mey J, Dräger UC (1996) Light-mediated retinoic acid production. Proc Natl Acad Sci U S A 93:12570–12574.

721 Medeiros NE, Curcio CA (2001) Preservation of ganglion cell layer neurons in age-related macular degeneration. Invest
722 Ophthalmol Vis Sci 42:795–803.

723 Meyer A, Hilgen G, Dorgau B, Sammler EM, Weiler R, Monyer H, Dedek K, Hormuzdi SG (2014) AII amacrine cells
724 discriminate between heterocellular and homocellular locations when assembling connexin36-containing gap
725 junctions. J Cell Sci 127:1190–1202.

726 Paik S-S, Park YS, Kim I-B (2020) Calcium- and Voltage-Dependent Dual Gating ANO1 is an Intrinsic Determinant of
727 Repolarization in Rod Bipolar Cells of the Mouse Retina. Cells 9:543.

728 Pfeiffer RL, Marc RE, Jones BW (2020) Persistent remodeling and neurodegeneration in late-stage retinal degeneration.
729 Prog Retin Eye Res 74:100771.

730 Polosukhina A, Litt J, Tochitsky I, Nemargut J, Sychev Y, De Kouchkovsky I, Huang T, Borges K, Trauner D, Van Gelder RN,
731 Kramer RH (2012) Photochemical restoration of visual responses in blind mice. Neuron 75:271–282.

732 Puthussery T, Gayet-Primo J, Taylor WR (2010) Localization of the Calcium-binding Protein Secretagogin in Cone Bipolar
733 Cells of the Mammalian Retina. J Comp Neurol 518:10.1002/cne.22234.

734 Roux S, Matonti F, Dupont F, Hoffart L, Takerkart S, Picaud S, Pham P, Chavane F (2016) Probing the functional impact of
735 sub-retinal prosthesis. eLife 5:e12687.

736 Sahel J-A, Boulanger-Scemama E, Pagot C, Arleo A, Galluppi F, Martel JN, Esposti SD, Delaux A, de Saint Aubert J-B, de
737 Montleau C, Gutman E, Audo I, Duebel J, Picaud S, Dalkara D, Blouin L, Taiel M, Roska B (2021) Partial recovery
738 of visual function in a blind patient after optogenetic therapy. Nat Med 27:1223–1229.

739 Scalabrino ML, Thapa M, Chew LA, Zhang E, Xu J, Sampath AP, Chen J, Field GD (2022) Robust cone-mediated signaling
740 persists late into rod photoreceptor degeneration. eLife 11:e80271.

741 Schilardi G, Kleinlogel S (2022) Two Functional Classes of Rod Bipolar Cells in the Healthy and Degenerated
742 Optogenetically Treated Murine Retina. Front Cell Neurosci 15:809531.

743 Schilardi G, Kralik J, Kleinlogel S (2023) Selective Block of Upregulated Kv1.3 Potassium Channels in ON-Bipolar Cells of
744 the Blind Retina Enhances Optogenetically Restored Signaling. Int J Mol Sci 24:14207.

745 Schindelin J, Arganda-Carreras I, Frise E, Kaynig V, Longair M, Pietzsch T, Preibisch S, Rueden C, Saalfeld S, Schmid B,
746 Tinevez J-Y, White DJ, Hartenstein V, Eliceiri K, Tomancak P, Cardona A (2012) Fiji - an Open Source platform for
747 biological image analysis. Nat Methods 9:10.1038/nmeth.2019.

748 Schmidt TM, Kofuji P (2011) An Isolated Retinal Preparation to Record Light Response from Genetically Labeled Retinal
749 Ganglion Cells. J Vis Exp:2367.

750 Schwartz GW, Okawa H, Dunn FA, Morgan JL, Kerschensteiner D, Wong RO, Rieke F (2012) The spatial structure of a
751 nonlinear receptive field. Nat Neurosci 15:1572–1580.

752 Sekirnjak C, Jepson LH, Hottowy P, Sher A, Dabrowski W, Litke AM, Chichilnisky EJ (2011) Changes in physiological
753 properties of rat ganglion cells during retinal degeneration. J Neurophysiol 105:2560–2571.

754 Shen N, Wang B, Soto F, Kerschensteiner D (2020) Homeostatic plasticity shapes the retinal response to photoreceptor
755 degeneration. Curr Biol 30:1916-1926.e3.

756 Singer JH, Diamond JS (2006) Vesicle depletion and synaptic depression at a mammalian ribbon synapse. J Neurophysiol
757 95:3191–3198.

758 Singer JH, Lassová L, Vardi N, Diamond JS (2004) Coordinated multivesicular release at a mammalian ribbon synapse. Nat
759 Neurosci 7:826–833.

760 Stasheff SF, Shankar M, Andrews MP (2011) Developmental time course distinguishes changes in spontaneous and light-
761 evoked retinal ganglion cell activity in rd1 and rd10 mice. J Neurophysiol 105:3002–3009.

762 Tachibana M, Okada T, Arimura T, Kobayashi K (1993) Dihydropyridine-sensitive calcium current mediates
763 neurotransmitter release from retinal bipolar cells. Ann N Y Acad Sci 707:359–361.

764 Telias M, Denlinger B, Helft Z, Thornton C, Beckwith-Cohen B, Kramer RH (2019) Retinoic Acid Induces Hyperactivity, and
765 Blocking Its Receptor Unmasks Light Responses and Augments Vision in Retinal Degeneration. Neuron.

766 Telias M, Sit KK, Frozenfar D, Smith B, Misra A, Goard MJ, Kramer RH (2022) Retinoic acid inhibitors mitigate vision loss in
767 a mouse model of retinal degeneration. Sci Adv 8:eabm4643.

768 Tetenborg S, Yadav SC, Hormuzdi SG, Monyer H, Janssen-Bienhold U, Dedek K (2017) Differential Distribution of Retinal
769 Ca2+/Calmodulin-Dependent Kinase II (CaMKII) Isoforms Indicates CaMKII-β and -δ as Specific Elements of
770 Electrical Synapses Made of Connexin36 (Cx36). Front Mol Neurosci 10:425.

771 Thapliyal S, Arendt KL, Lau AG, Chen L (2022) Retinoic acid-gated BDNF synthesis in neuronal dendrites drives
772 presynaptic homeostatic plasticity. eLife 11:e79863.

773 Tien N-W, Soto F, Kerschensteiner D (2017) Homeostatic plasticity shapes cell-type-specific wiring in the retina. Neuron
774 94:656-665.e4.

775 Tochitsky I, Helft Z, Meseguer V, Fletcher RB, Vessey KA, Telias M, Denlinger B, Malis J, Fletcher EL, Kramer RH (2016)
776 How azobenzene photoswitches restore visual responses to the blind retina. Neuron 92:100–113.

777 Tochitsky I, Polosukhina A, Degtyar VE, Gallerani N, Smith CM, Friedman A, Van Gelder RN, Trauner D, Kaufer D, Kramer
778 RH (2014) Restoring visual function to blind mice with a photoswitch that exploits electrophysiological
779 remodeling of retinal ganglion cells. Neuron 81:800–813.

780 Trenholm S, Awatramani GB (2015) Origins of spontaneous activity in the degenerating retina. Front Cell Neurosci 9:277.

781 Turano K, Wang X (1992) Motion thresholds in retinitis pigmentosa. Invest Ophthalmol Vis Sci 33:2411–2422.

782 von Gersdorff H, Matthews G (1997) Depletion and Replenishment of Vesicle Pools at a Ribbon-Type Synaptic Terminal. J
783 Neurosci 17:1919–1927.

784 Wan Q-F, Heidelberger R (2011) Synaptic Release at Mammalian Bipolar Cell Terminals. Vis Neurosci 28:109–119.

785 Weingarten DJ, Shrestha A, Juda-Nelson K, Kissiwaa SA, Spruston E, Jackman SL (2022) Fast resupply of synaptic vesicles
786 requires synaptotagmin-3. Nature 611:320–325.

787 Yadav SC, Tetenborg S, Dedek K (2019) Gap Junctions in A8 Amacrine Cells Are Made of Connexin36 but Are Differently
788 Regulated Than Gap Junctions in AII Amacrine Cells. Front Mol Neurosci 12:99.

789 Zhu Y, Xu J, Hauswirth WW, DeVries SH (2014) Genetically Targeted Binary Labeling of Retinal Neurons. J Neurosci
790 34:7845–7861.

791 Zucker RS, Regehr WG (2002) Short-term synaptic plasticity. Annu Rev Physiol 64:355–405.

792